RESEARCH MEMORANDUM

EFFECTS OF REYNOLDS NUMBER ON THE AERODYNAMIC CHARACTERISTICS OF A DELTA WING AT MACH NUMBER OF 2.41

By John E. Hatch, Jr., and L. Keith Hargrave

Langley Aeronautical Laboratory
Langley Field, Va.

NATIONAL ADVISORY COMMITTEE
FOR AERONAUTICS

WASHINGTON

October 22, 1951

(Classification cancelled or changed to Unclassified)

By authority of NASA Tech Pub Announcement #105

(NAME OF PERSON AUTHORIZED TO CHANGE)

20 Aug 62

By NK

GRADE OF OFFICER MAKING CHANGE)

5 Apr 62

DATE

[redacted]

ERRATA NO. 1

NACA RM L51H06

EFFECTS OF REYNOLDS NUMBER ON THE AERODYNAMIC CHARACTERISTICS OF A DELTA WING AT MACH NUMBER OF 2.41

By John E. Hatch, Jr., and L. Keith Hargrave

October 22, 1951

Figure 15 of this paper is in error and should be replaced with new figure 15 attached. This change also requires a revision in the text as follows:

Pages 13 and 14: Replace the last sentence beginning on page 13 and continuing on page 14 with the two following sentences:

"Up to about 10° angle of attack the spanwise load distribution was reasonably independent of Reynolds number. Outboard of the 40 percent semispan station of the wing at 10° angle of attack the experimental spanwise loading coefficients were considerably lower than predicted by the linear theory."

[redacted]

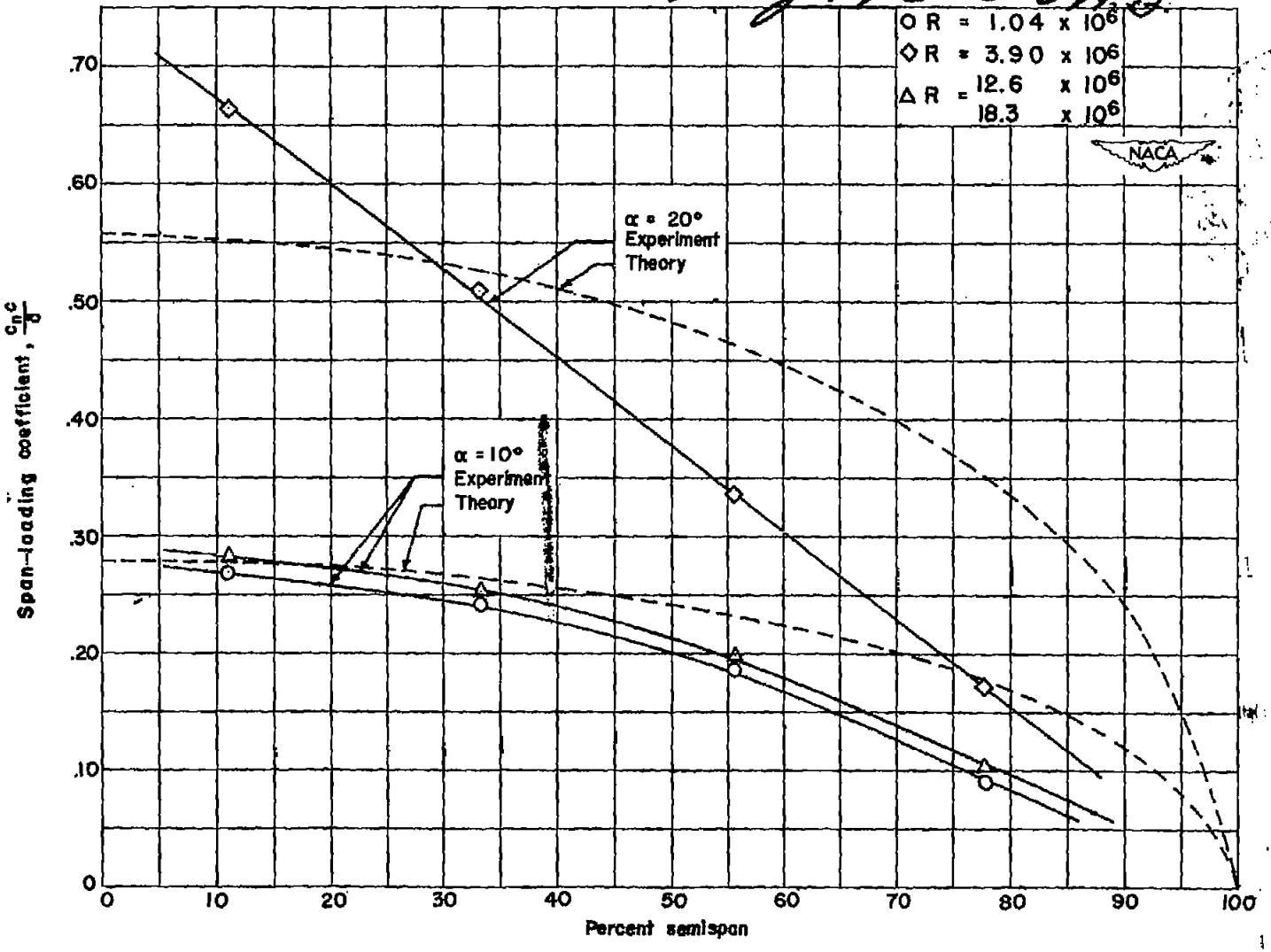

Figure 15.- Comparison of theoretical and experimental spanwise load distribution at different Reynolds numbers.

NATIONAL ADVISORY COMMITTEE FOR AERONAUTICS

RESEARCH MEMORANDUM

EFFECTS OF REYNOLDS NUMBER ON THE AERODYNAMIC CHARACTERISTICS OF A DELTA WING AT MACH NUMBER OF 2.41

By John E. Hatch, Jr., and L. Keith Hargrave

SUMMARY

The results of an experimental investigation to determine the effects of Reynolds number on the flow characteristics over a delta wing at a Mach number of 2.41 are presented. The wing streamwise airfoil sections are based on the NACA 00-thickness series with the maximum thickness varying from 4 percent at the root section to 6.24 percent at the 90-percent spanwise station.. Force and pressure data for similar models having an aspect ratio of 1.57 were obtained over an angle-of-attack range at Reynolds numbers of 1.04×10^6, 3.9×10^6, 12.6×10^6, and 18.3×10^6.

The results showed negligible effects of a Reynolds number variation of 1.04×10^6 to 18.3×10^6 on the measured force characteristics over an angle-of-attack range from 0° to 6°. For angles of attack from 6° to 20°, and increase of Reynolds number from 12.6×10^6 to 18.3×10^6. likewise had no effect on the force data.

The results did show, however, a definite effect of Reynolds number on the flow and load distribution over the wing at angles of attack. On the upper surface an increase in Reynolds number from 1.04×10^6 to 12.6×10^6 delayed the formation of a separated region near the leading edge which terminated in a shock wave along a ray through the wing apex. On the wing lower surface the pressure coefficients over the forward 30 percent of the wing were increased as the Reynolds number varied from 1.04×10^6 to 12.6×10^6. Because of the compensating changes in the upper-surface pressure distribution, the lift coefficients did not change with Reynolds number through an angle of attack of 6° as verified by the force data. As the Reynolds number was further increased from 12.6×10^6 to 18.3×10^6 no effect on the wing pressure distribution was evident.

[redacted]

INTRODUCTION

Much wind-tunnel test data on delta wings is now available. Various plan forms using many different airfoil sections have been tested over a range of supersonic Mach numbers up to about $M = 3$. Most tests, however, have been conducted at Reynolds numbers much lower than those realized by full-scale wings. The present investigation was undertaken to determine the effects of a large variation of Reynolds number $(1.04 \times 10^6$ to $18.3 \times 10^6)$ on the aerodynamic characteristics of a delta wing and is believed to be the first such comparison made for one wing at supersonic speeds over such a wide Reynolds number range. Another purpose of the investigation was to provide high Reynolds number data for the wing at angles of attack up to 20°. A test Reynolds number of 18.3×10^6 corresponds to a wing with a mean aerodynamic chord of 10 feet at an altitude of 60,000 feet and a Mach number of 2.41.

The high Reynolds number data $(R = 12.6 \times 10^6$ and $18.3 \times 10^6)$ were obtained in a Langley 9-inch blowdown jet of the Gas Dynamics Branch, and the low Reynolds number data were obtained in the Langley 9-inch supersonic tunnel. A description of the jet and the jet calibration are presented in the appendix of this paper.

SYMBOLS

Free-stream conditions:

ρ	mass density of air
V	stream velocity
a	speed of sound
M	Mach number (V/a)
q_o	dynamic pressure $\left(\frac{1}{2}\rho V^2\right)$
p_o	static pressure
R	Reynolds number, based on wing mean aerodynamic chord

Wing geometry:

S	plan form

b span

c wing chord, measured in direction of flight

$\bar{c}$ mean aerodynamic chord $\left(\int_0^{b/2} c^2 dy \Big/ \int_0^{b/2} c\ dy\right)$

t thickness

α angle of attack, degrees

x coordinate along free-stream condition

y spanwise coordinate

Pressure data:

p local static pressure

C_p pressure coefficient $\left(\frac{p - p_o}{q_o}\right)$

$\Delta p/q_o$ lifting-surface pressure coefficient per degree angle of attack $\left(\frac{p_l - p_u}{q_o}\right)$

$c_n c/\bar{c}$ span-loading coefficient $\left(\int_0^c \frac{C_p}{\bar{c}}\, dc\right)$

Force data:

C_L wing-lift coefficient $\left(\frac{\text{Lift}}{q_o S}\right)$

C_D wing-drag coefficient $\left(\frac{\text{Drag}}{q_o S}\right)$

C_M wing pitching-moment coefficient about wing centroid of area $\left(\frac{\text{Pitching Moment}}{q_o S \bar{c}}\right)$

$\frac{L}{D}$ lift-drag ratio

ΔC_D incremental-drag coefficient due to lift $(C_D - C_{D_{min}})$

Subscripts:

u conditions on wing upper surface

l conditions on wing lower surface

r value at root section

max maximum value

min minimum value

DESCRIPTION OF APPARATUS

Blowdown Jet

Jet.- The high-Reynolds-number tests were conducted in a Langley M = 2.41 blowdown jet having a rectangular test section, 9 inches wide and $5\frac{3}{4}$ inches high. A drawing showing the general arrangement of the jet is presented in figure 1. A boundary-layer scoop, which exhausts to the atmosphere, is used to remove the boundary layer from just in front of the floor-mounted, semispan wing model. The jet has parallel sidewalls and had viewing windows covering the entire test section.

By varying the stagnation pressure in the settling chamber from 100 pounds per square inch absolute to 145 pounds per square inch absolute, the Reynolds number was varied from 12.6×10^6 to 18.3×10^6. The final Mach number distribution in the jet test section is presented in figure 2. In this figure the wing model apex at an angle of attack of 0° is located at station 1.5 and the trailing edge is at station 11.5. The lip of the boundary-layer scoop is at station 1.0. A more complete description of the jet is given in the appendix.

Wing model.- The semispan wing models having an aspect ratio of 1.57 were constructed from steel. Streamwise airfoil sections are based on the NACA 00-thickness series which has its maximum thickness at 30 percent of the chord. The leading-edge radii were modified to average about 0.4 percent of the local chord. As shown in figure 3(a), the measured wing maximum thickness varies from 4 percent at the root to 6.24 percent at the 90-percent semispan station. A typical section is shown in figure 3(b).

Structural considerations required two pressure models in order to include all the desired pressure orifices (orifice locations tabulated in table I). Each wing had two rows of chordwise pressure orifices which resulted in four spanwise pressure stations for the basic wing. Figure 4 shows the semispan wing geometry and the locations of the chordwise pressure stations. A third model was constructed for the force tests. Each model was constructed to within ±0.001 inch of the specified ordinates.

Langley 9-Inch Supersonic Tunnel

Tunnel.- The low Reynolds number data were obtained in the Langley 9-inch supersonic tunnel. This tunnel is a single-return, direct-drive type in which the pressure and humidity of the enclosed air can be controlled. The tunnel has recently been repowered and the stagnation pressure can now be regulated between 0.2 and 4.3 atmospheres at a Mach number of 2.41. A Mach number distribution in the test section of 2.41 ± 0.015 was determined for the stagnation pressure range of 1 to 4 atmospheres. Throughout the tests the amount of water vapor in the tunnel air was kept at sufficiently low values to insure negligible effects of condensation in the test section.

Wing model and support system.- The full-span model was constructed of brass. The section shapes varied slightly from those of the semispan model due to fabrication error (see fig. 3). After the force tests were completed, pressure tubes were installed in the model along the same spanwise stations as those in the semispan model.

As shown in figure 5, the full-span model was mounted from the rear on a very slender tapered sting support. An identical support arrangement is described in detail in reference 1 in which tests were made to determine the lift and drag of the sting alone. It was found that the lift force was negligible, and that the drag force was almost constant with angle of attack. At a Mach number of 2.41 the sting gave a drag coefficient of approximately 0.0005 based on the wing area of the present tests. The magnitude of the drag coefficient contributed by the sting to the wing-sting combination is doubtful, but it was probably somewhat less than the 0.0005 value since some of the frontal area of the sting was buried in the wing and most of the sting was immersed in the boundary-layer flow of the wing.

TESTS AND PRECISION

Force measurements on the semispan model were obtained by a three-component strain-gage balance system over an angle-of-attack range from 0° to 20° in increments of 2°. Pressure data were also obtained at the same angles at a Reynolds number of 12.6×10^6, but the maximum angle of attack obtainable was 16° at a Reynolds number of 18.3×10^6. Both force and pressure data were recorded photographically.

Since pressure orifices were installed on only one surface of each wing, the models were set at positive and negative angles of attack in order to obtain pressures on both the upper and lower surfaces at any one angle of attack.

Pressure data for the full-span model were obtained over an angle-of-attack range from 0° to 10° in increments of 2°. Force data were obtained for angles of attack from 0° to 6° in increments of 1°. The angle of attack was obtained by initially referencing the wing in the tunnel with respect to the tunnel center line and then using an optical system for relative angles of attack.

The liquid-film method was used in the low Reynolds number tests to supplement the pressure distributions in the study of the flow over the wing. This method was the same as that used and described in reference 1. The model was given a black finish before applying the liquid film solution. Upon completion of a run, the wing was dusted with white powder. Accordingly, the wet (low shear) regions appear white and the dry (high shear) regions remain black.

In order to compare the force data for the wing-sting combination with the force data for the floor-mounted semispan model, it was necessary to correct the full-span model drag coefficient to account for the base drag of the sting. The pressure in the movable windshield and balance box was controlled at approximately free-stream pressure; therefore, the base drag correction was very small.

Because of the presence of the pressure tubes downstream of and near the trailing edge of the wing, the pressure readings for the orifices located 5 percent of the root chord from the trailing edge are of doubtful accuracy.

To understand better the wing-flow characteristics, a method was devised to determine the local flow direction over the upper surface of the full-span wing at angles of attack. Small, symmetrical, free-floating vanes were installed on the full-span wing at 15 different locations. Figure 6 shows the physical dimensions of the vanes as well

as the vane locations on the wing surface. The vanes were so located on the wing during each run that no interference effects between vanes were possible.

The angles through which the vanes were turned at each wing angle of attack were read by means of a cathetometer mounted outside of the tunnel. The accuracy of measurement of the indicated flow angles is estimated at $\pm\frac{1}{2}^{\circ}$.

The estimated probable error in the aerodynamic coefficients for the two models are as follows:

Model	α (deg)	C_L	C_D	C_M	C_p	R	M
Full Span	-----	±0.0002	±0.0002	±0.0002	±0.0050 ±0.0015	1.04×10^6 3.90×10^6	2.41 ± 0.015
Semispan	±0.10	±0.0030	±0.0006	±0.0003	±0.0040 ±0.0026	12.6×10^6 18.3×10^6	

The probable error in angle of attack of the full-span wing is $\pm 0.07^{\circ}$ in the initial reference of the model with respect to the tunnel center line and $\pm 0.03^{\circ}$ in relative angle of attack.

RESULTS AND DISCUSSION

Force Data

A comparison of the force data for the semispan, floor-mounted wing at Reynolds numbers of 12.6×10^6 and 18.3×10^6 with the data for the full-span, sting-supported model at a Reynolds number of 1.04×10^6 is presented in figure 7. The theoretical lift curve as determined from the linear theory is plotted for comparison. Pitching moments are taken about the centroid of plan-form area, with the wing mean aerodynamic chord as the reference length. Within experimental accuracy, the force data at negative angles of attack and positive angles of attack are the same. As a result, only the data for positive angles of attack are shown.

Lift.- The experimental lift curve for the high Reynolds number tests is linear up to about an angle of attack of 10°. From angles of

attack of 10° to 20°, there is a slight decrease in the lift-curve slope. The low Reynolds number tests also show the linearity of the lift curve up to an angle of attack of 6°, the extent of the test range. The experimental lift-curve slope through zero lift is about 0.025 per degree; whereas the theoretical value of the lift-curve slope calculated by the method of reference 2 is 0.0295 per degree.

A comparison of the wing-lift curves at the two Reynolds numbers indicates that, within the experimental accuracy of the tests, the Reynolds number has no effect on the wing-lift coefficients over the angle-of-attack range covered by the comparison, 0° to 6°.

Pitching moment.- The pitching-moment coefficients as shown are taken about the wing center of area. Through the common range of angle of attack, 0° to 6°, the data obtained at the two test Reynolds numbers are approximately the same and indicate a center-of-pressure location close to the center of wing area which agrees with theory. The data obtained at the Reynolds numbers of 12.6×10^6 and 18.3×10^6 for an angle of attack from 6° to 20° show a forward shift of the center of pressure with increasing lift. At an angle of attack of 20°, the center of pressure moved to a point 3.4 percent of the mean aerodynamic chord ahead of the wing center of area.

Drag.- Within the experimental accuracy of the test procedures, the wing-drag data obtained at each Reynolds number agreed over the common angle-of-attack range from 0° to 6°. Over the complete angle-of-attack range for the tests at both Reynolds numbers, the drag-rise factor $\Delta C_D/C_L^2$ is approximately equal to the reciprocal of the lift-curve slope and implies practically no leading-edge suction force.

A minimum drag coefficient of 0.0095 was obtained from both tests. It would be expected that a lower minimum drag coefficient would be obtained from the tests at a Reynolds numbers of 1.04×10^6 than from the high Reynolds number tests since the flow over the wing will be largely laminar at the low Reynolds number; whereas turbulent flow would probably exist over most of the wing at a Reynolds number of 18.3×10^6. In order to compare the two minimum drag-coefficient values, however, the contribution of the sting to the full-span-configuration drag coefficient (approx. 0.0004) would have to be substracted from the 0.0095 value.

A wing pressure drag coefficient at zero lift of 0.0058 was determined from the high Reynolds number pressure-distribution data. Subtraction of this value from the minimum drag coefficient gives a friction-drag coefficient of 0.0037. This result compared with a value of 0.0040 for the compressible turbulent friction-drag coefficient as obtained from extrapolated experimental data of reference 3.

Less complete low Reynolds number pressure-distribution data estimates the same pressure drag coefficient at zero lift as that obtained from the high Reynolds number data. Subtraction of this value and the 0.0004 sting contribution from the minimum drag coefficient gives a friction-drag coefficient of 0.0033 for the wing at a Reynolds number of 1.04×10^6. This value compares with an incompressible skin-friction coefficient of 0.0026. The larger experimental viscous drag coefficient could be the result of separated flow, a small region of turbulent flow, or a higher than estimated sting drag contribution.

Lift-drag ratio.- A maximum lift-drag ratio of 6.4 was obtained by the wing at an angle of attack of approximately 5°.

From a comparison of the force data obtained for the wing at Reynolds numbers of 1.04×10^6 and 18.3×10^6, it is evident that Reynolds number has little effect on the wing-force coefficients over the angle-of-attack range covered by the comparison, 0° to 6°.

Pressure-Distribution Data

The greatest effects of Reynolds number on the aerodynamic data for this delta wing were found in the pressure distributions. Although differences in the pressure distribution were readily apparent as the Reynolds number varied from 1.04×10^6 to 12.6×10^6, the pressure data were the same for Reynolds numbers of 12.6×10^6 and 18.3×10^6 up to angles of attack of 16°. Only representative data which show the effects of Reynolds number are plotted in this paper. Complete pressure data for the wing at each angle of attack for each Reynolds number investigated, however, are presented in table I.

Upper Surface.- The data of the present investigation show the presence of spanwise pressure discontinuities on the wing upper surface beginning at about an angle of attack of 4° at a Reynolds number of 1.04×10^6 and at about an angle of attack of 10° at a Reynolds number of 12.6×10^6 and 18.3×10^6.

For example, figure 8 shows the spanwise variation of pressure coefficient at the 90-percent root-chord station. At an angle of attack of 6°, the data for a Reynolds number of 1.04×10^6 show that a separated region of approximately constant negative pressure exists near the leading edge which terminates in an abrupt pressure jump at about the 40-percent semispan station. The high Reynolds number data indicate no such pressure discontinuity at this angle of attack. As the angle of attack is increased to 10°, however, the pressure jump occurs even at the highest

Reynolds number. From other spanwise pressure plots taken at different chordwise stations it is possible to determine that the pressure jump, which exists on the upper surface, lies approximately along the ray $\frac{y}{x} = 0.17$.

The strong resemblance of the present pressure data to that of reference 4 indicates that the pressure discontinuities could be the result of shock waves on the upper surface of the wing. Unpublished work by Clinton E. Brown of the Langley Laboratory indicated the existence of shock waves on the upper surface of delta wings at angles of attack even when the leading edge is swept well behind the Mach cone. The data of reference 5 also show the existence of shock waves normal to the wing surface, but oblique to the supersonic stream.

In the present investigation, if the jump in pressure were caused by a shock wave then the component of local Mach number normal to the ray along which the pressure jump lies would have to be supersonic. The results of the vane survey showed that, for wing angles of attack of 6°, 8°, and 10°, the flow over the upper surface was turned toward the root chord a sufficient amount to result in the component of flow normal to the ray $\frac{y}{x} = 0.17$ to be supersonic. It was therefore concluded that the pressure discontinuity on the present wing represented a shock wave.

The vane-survey results at a wing angle of attack of 10° and a Reynolds number of 1.04×10^6 are shown in figure 6. The table (fig. 6) gives, for each vane location, the angle in degrees through which the flow is turned from the free-stream direction and the local Mach number as computed from the pressure data. Positive angles indicate that the flow is turned toward the root chord. Local Mach numbers at vane positions 2 and 5 could not be calculated because of the absence of pressure tubes in the vicinity of these vane positions. The vectors at vane positions 2 and 5 are, therefore, shown by dashed lines. Figure 6 further shows that behind the shock wave the vanes indicate that the flow has turned back to a direction approximately parallel to the free stream.

It may be noted from figure 6 that the vanes were mounted 0.125 inch above the wing surface. This 0.125-inch height was selected as a result of systematic tests to determine the effect of the height of the vane above the wing surface on the indicated flow angles. When mounted 0.07 inch above the wing surface the vanes were well in the wing boundary layer, and for angles of attack above 6° the vanes outboard of the ray $\frac{y}{x} = 0.17$ indicated that the flow in the boundary layer was turned away from the root chord toward the low-pressure area at the wing tip.

When raised to a height of 0.125 inch above the wing, the vanes indicated that the flow outboard of the ray $\frac{y}{x} = 0.17$ was turned toward the root chord. As the height was increased further to 0.30 inch, the indicated flow angle was somewhat less than the maximum indicated flow angle. It is not expected that one particular vane height above the wing surface will give the true flow direction at each vane location. It was felt, however, that the 0.125-inch height, in general, gave a good indication of the flow direction over the wing surface.

The variation of the indicated flow angles across the span at the 70-percent root-chord station with wing angle of attack is shown in figure 9(a), and figure 9(b) shows the vane locations on the wing profile at the 70-percent root-chord station. It is significant that the abrupt change in the indicated flow angles occurs at the location of the ray along which the pressure discontinuity occurs. Insufficient pressure data across the span at this station, however, does not permit a complete correlation of pressure data and vane-survey data.

At each chordwise station the formation of the shock wave along the ray $\frac{y}{x} = 0.17$ was delayed to a higher angle of attack with each increase in Reynolds number. As the angle of attack was increased to 16° at high Reynolds numbers, the shock wave continued to exist but, as shown by figure 10, its location moved inboard with each increasing angle of attack. As the angle of attack was increased to 20°, the presence of the shock wave is no longer evident at the 90-percent-root-chord station. Spanwise pressure distributions at the 60-percent and 70-percent root-chord stations, however, show that even at an angle of attack of 20° a shock wave continues to exist on the wing, but its inboard movement with angle of attack stops at about $\alpha = 16°$.

Liquid-film pictures taken at a Reynolds number of 1.04×10^6 are presented in figure 11 to further show the location and development of the pressure jump on the upper surface of the wing. As the wing angle of attack is increased from 0° to 10° the development of the disturbance (high shear) area is evident.

It has been indicated in reference 5 that the formation of a similar shock wave on the upper surface of two delta wings investigated at supersonic speeds was primarily a function of the Mach number of the flow component perpendicular to the swept leading edge and the shape of the airfoil in the vicinity of the wing leading edge. The data of the present investigation, however, show that the formation of the shock wave also varies with Reynolds number and is, therefore, greatly dependent upon viscous effects.

[redacted]

This shock-wave formation on the surface of delta wings appears to be very complex and probably involves several variables, such as, leading-edge profile, Mach number, Reynolds number, and thickness distribution. At the present time, no single variable is known to be the controlling factor in the formation of the shock wave.

Examination of chordwise plots of the pressure data at Reynolds numbers of 12.6×10^6 and 18.3×10^6 shows the presence of a curved shock wave near the wing leading edge lying essentially along the ray $\frac{y}{x} = 0.3$. The shock wave is first formed at about $\alpha = 6^\circ$ and exists up to a wing angle of attack of 12°. Above an angle of attack of 12° the presence of this shock wave is no longer evident. The data obtained at a Reynolds number of 1.04×10^6 does not show the presence of the shock wave through an angle of attack of 10°. At a Reynolds number of 3.9×10^6 the existence of the shock wave is evident only at an angle of attack of 6°. The effects of Reynolds number on this shock-wave formation near the leading edge is not clear since the upper-surface pressure distribution over the wing near the leading edge does not consistently vary with Reynolds number.

Since a large change in Reynolds number changed the flow characteristics over the wing, any downwash survey made behind the wing would be affected by a large variation in Reynolds number. It would also be expected that the effectiveness of control surfaces located at the tip and at the trailing edge would vary with a large Reynolds number change since the separated region first begins at the tip and moves toward the wing apex and root chord with increasing angle of attack.

Lower surface.- On the wing lower surface there was also found a definite variation of pressure distribution with a change in Reynolds number. Figure 12 shows the chordwise variation of pressure coefficients for the 55.5-percent semispan station for angles of attack of 2°, 6°, and 10° at each Reynolds number. Forward of about the 30-percent-chord station, the pressure-distribution curves are shifted in a positive direction as the Reynolds number is increased from 1.04×10^6 to 12.6×10^6. As the Reynolds number was further increased to 18.3×10^6 no additional displacement of the curves is evident. The displacement of the lower-surface pressure-coefficient curves indicates that the section stagnation point moves rearward with an increase in Reynolds number. The increase in pressure coefficient over the forward part of the lower surface alone would result in a higher lift coefficient at any angle of attack for the high Reynolds number tests. Because of the compensating changes in the upper-surface pressure distribution, however, the lift coefficients did not vary with Reynolds number through the compared angle-of-attack

range of 0° to 6°, as verified by the force data. From about the 30-percent-local-chord station to the trailing edge, the pressure-distribution curves for the wing lower surface show no significant difference for the different Reynolds numbers.

It is felt that the changes in pressure distribution which occur with a change in Reynolds number are not a result of elastic deformation of the different models due to air loads. If the wing models had deflected, the chordwise pressure distributions on both the upper and lower surfaces would be affected. On the wing lower surface through a wing angle of attack of 10° the pressure distribution varies only over approximately the forward 30 percent of the airfoil, as shown by figure 12. Over the remaining 70 percent of the airfoil where the greatest deformation should occur (the thinnest part of the wing), the pressure distributions are about the same for each Reynolds number for any one angle of attack. It was, therefore, concluded that the differences in pressure distribution which existed with a change in Reynolds number were not a result of elastic deformation of the wing.

Loading.- Since differences have been shown to exist for the upper- and lower-surface pressure distributions as a result of a large variation of Reynolds number, it is of interest to determine the effects of Reynolds number on the over-all loading of the wing. Figure 13 shows the distribution of experimental loading coefficients per degree angle of attack for $\alpha = 10°$. At the 11.1-percent semispan station the loading coefficients at a Reynolds number of 1.04×10^6 indicate an abrupt decrease in loading at the position of the shock wave which exists on the wing upper surface; whereas the loading for the other Reynolds numbers at this station show good agreement over the entire chord. The influence of the shock wave on the loading coefficients at the 33.3-percent semispan station is evident by the sudden decrease in loading at about the 65-percent-chord station. At the 33.3 and 55.5-percent semispan stations there is a definite trend of higher loading coefficients with an increase in Reynolds number over about the forward 30 percent of each station. In moving outboard to the 77.7-percent semispan station the same general trend of higher loading coefficients with increasing Reynolds number is again evident, but the differences are small and occur over the rearward part of the chord.

As the angle of attack was increased from 10° to 20° the loading coefficients at high Reynolds numbers varied as shown in figure 14.

The departure from theory of the over-all experimental loading at high angles of attack is presented in figure 15, which shows the variation of span-loading coefficient as obtained from the integrated pressure distribution at each chordwise station. Up to about 10° angle of attack the spanwise load distribution ~~agreed fairly well with the~~ WAS REASONABLY INDEPENDENT

of REYNOLDS NUMBER. Outboard of the 40 percent linearized theory at each Reynolds number even though differences were found to exist with Reynolds number at each spanwise station. At higher angles of attack the loading across the span continued to depart from theory until at an angle of attack of 20° the variation of section normal-force coefficient became practically linear. This linear variation of spanwise loading at high angles of attack has also been observed in unpublished data obtained from the Langley 9-inch supersonic tunnel for a delta wing composed of symmetrical double-wedge sections, 10 percent thick, investigated at angles of attack from 0° to 52°, at M = 2.41, and a Reynolds number of 520,000. From these investigations it would seem that, for delta wings at high angles of attack, airfoil shape and thickness distribution has practically no effect on the spanwise load distribution.

CONCLUSIONS

From the experimental investigation to determine the effects of Reynolds number on the flow characteristics over a delta wing at a Mach number of 2.41 the following conclusions may be made:

1. Over an angle-of-attack range from 0° to 6° a change in Reynolds number from 1.04×10^6 to 18.3×10^6 had no significant effects on the measured force characteristics. For angles of attack from 6° to 20° an increase in Reynolds number from 12.6×10^6 to 18.3×10^6 likewise had no effect on the force data.

2. The results did show, however, a definite effect of Reynolds number on the flow over the wing at angles of attack. On the upper surface an increase in Reynolds number from 1.04×10^6 to 12.6×10^6 delayed to a higher angle of attack the formation of a separated region near the leading edge which terminated in a shock wave along a ray through the wing apex. As the angle of attack was increased to 20° at high Reynolds numbers the shock wave continued to exist.

3. On the lower surface the pressure coefficients over the forward 30 percent of the wing were increased as the Reynolds number varied from 1.04×10^6 to 12.6×10^6. Because of the compensating changes in the upper-surface pressure distribution the measured lift coefficients did not vary with Reynolds number through the compared angle-of-attack range of 0° to 6°.

4. For an angle-of-attack range from 0° to 16°, an increase in Reynolds number from 12.6×10^6 to 18.3×10^6 had no effect on the wing pressure distribution.

Langley Aeronautical Laboratory
National Advisory Committee for Aeronautics
Langley Field, Va.

[redacted]

APPENDIX

DESCRIPTION OF BLOWDOWN JET

The supersonic nozzle section of the jet was designed by the method of characteristics to produce a uniform flow at $M = 2.41$ in the test section. Boundary-layer displacement thickness along the supersonic nozzle was computed by the method of reference 6. The same boundary-layer displacement thickness was assumed to exist along the sidewalls, and the combined boundary-layer correction was applied to the theoretical nozzle ordinates.

Strain-gage balance system.- Force data were obtained by a three-component strain-gage balance system. The balance system rotated with the wing model and at each angle of attack measured normal force, chord force, and pitching moment. The pitching moment was measured about the 50-percent root-chord station.

The balance was temperature-compensated and calibrated to determine interaction effects between components. Interaction effects were so small that they could not be recorded on the scales. Each force component on the balance was transmitted to a separate single-channel self-balancing Brown potentiometer. The force data were recorded photographically.

Angle-of-attack mechanism.- The floor-mounted models were attached to a turntable which was rotated over a wing angle-of-attack range of $\pm 20^\circ$ by a remotely-controlled electric motor. The wing angle of attack was measured by means of an electrical slide wire resistor attached to the turntable transmitting its reading to a single-channel self-balancing Brown potentiometer. Each angle of attack was checked by means of a protractor assembly mounted on the jet test section and turntable. Before each series of tests, the zero angle of attack was carefully estabilished from a previously determined reference plane.

JET CALIBRATION

The Mach number distribution throughout the jet test section was determined by means of a static tube rake survey. The rake was so mounted that the five static tubes were in a vertical plane. A survey was made along the test-section center line (in increments of 1 in.) as well as along one transverse station $2\frac{1}{4}$ inches on each side of the jet center line. At each station the Mach number was determined

from the ratio of free-stream static pressure to the settling-chamber stagnation pressure.

The final test-section Mach number distribution is shown in figure 2. In front of the shock wave formed by the boundary-layer scoop, the Mach number is 2.43 ± 0.01, and behind the shock wave caused by the scoop (in the region occupied by the wing model) the Mach number is 2.41 ± 0.015. Uniform flow existed in the test section for a distance of 13 inches. The jet calibration was conducted at a stagnation pressure of 115 pounds per square inch absolute which would result in a Reynolds number of 2.17×10^6 per inch.

All calibration tests were conducted in a range of stagnation dewpoints which eliminated any effect of condensation.

During the jet calibration, a disturbance was found to originate at the joint between the turntable and the test-section floor, even though the maximum difference in level between the two surfaces was approximately ±0.002. The disturbance caused a change in Mach number of ±0.03 in the test section and was detected by the static rake during the longitudinal survey of the jet. The disturbance was eliminated by spraying the jet floor and turntable with surfacing putty and polishing the resulting continuous surface to a high gloss. The smoothness of the surface was maintained during all calibration tests and wing tests.

Throughout the testing program the scoop edge was kept sharpened to a knife edge to reduce the strength of the shock wave formed at the lip of the scoop. From the jet calibration, it was determined that the loss in Mach number across the shock wave at the scoop is 0.02.

REFERENCES

1. Love, Eugene S.: Investigations at Supersonic Speeds of 22 Triangular Wings Representing Two Airfoil Sections for Each of 11 Apex Angles. NACA RM L9D07, 1949.

2. Brown, Clinton E.: Theoretical Lift and Drag of Thin Triangular Wings at Supersonic Speeds. NACA Rep. 839, 1946. (Formerly NACA TN 1183)

3. Wilson, R. E., Young, E. C., and Thompson, M. J.: 2nd Interim Report on Experimentally Determined Turbulent Boundary-Layer Characteristics at Supersonic Speeds. CM 501, The John Hopkins Univ. Appl. Phys. Lab., Jan. 1949. (Univ. Texas, Defense Research Lab.)

4. Daley, Bernard N., and Lord, Douglas R.: Aerodynamic Characteristics of Several 6-Percent-Thick Airfoils at Angles of Attack from 0° to 20° at High Subsonic Speeds. NACA RM L9E19, 1949.

5. Boyd, John W., and Phelps, E. Ray: A Comparison of the Experimental and Theoretical Loading over Triangular Wings at Supersonic Speeds. NACA RM A50J17, 1951.

6. Tetervin, Neal: Approximate Formulas for the Computation of Turbulent Boundary-Layer Momentum Thicknesses in Compressible Flows. NACA ACR L6A22, 1946.

TABLE I.-EXPERIMENTAL PRESSURE COEFFICIENTS

$R = 1.04 \times 10^6$

Station		$\alpha = 0°$	$\alpha = 2°$		$\alpha = 4°$		$\alpha = 6°$		$\alpha = 8°$		$\alpha = 10°$	
$\frac{y}{b/2}$	Percent c	C_p	C_{p_u}	C_{p_l}	C_{p_u}	C_{p_l}	C_{p_u}	C_{p_l}	C_{p_u}	C_{p_l}	C_{p_u}	C_{p_l}
0.111	4.7	0.0400	0.0071	0.0635	-0.0200	0.0941	-0.0459	0.1305	-0.0823	0.1622	-0.1105	0.1952
	8.6	.0259	-.0047	.0506	-.0259	.0788	-.0506	.1093	-.0799	.1423	-.1164	.1740
	15.5	.0024	-.0223	.0235	-.0400	.0506	-.0658	.0788	-.0870	.1093	-.1282	.1423
	22.7	-.0059	-.0306	.0118	-.0470	.0388	-.0670	.0658	-.0858	.0941	-.0788	.1270
	33.7	-.0129	-.0329	.0082	-.0506	.0317	-.0670	.0564	-.0823	.0858	-.0811	.1187
	45.4	-.0188	-.0400	-.0012	-.0553	.0223	-.0647	.0459	-.0764	.0729	-.0835	.1035
	56.6	-.0188	-.0400	-.0012	-.0541	.0235	-.0647	.0482	-.0741	.0741	-.0894	.1011
	67.7	-.0188	-.0494	.0012	-.0541	.0223	-.0647	.0459	-.0741	.0717	-.0917	.1011
	83.1	-.0282	-.0506	-.0106	-.0623	.0094	-.0729	.0317	-.0811	.0553	-.0952	.0847
	94.3	-.0447	-.0647	-.0270	-.0752	-.0082	-.0870	.0118	-.0941	.0341	-.1046	.0611
0.333	5.3	0.0247	-0.0176	0.0564	-0.0506	0.0917	-0.0999	0.1258	-0.1364	0.1575	-0.1564	0.1893
	14.7	-.0165	-.0517	.0106	-.0776	.0435	-.1011	.0741	-.1305	.1070	-.1528	.1411
	23.8	-.0235	-.0541	0	-.0776	.0306	-.1011	.0600	-.1364	.0905	-.1575	.1234
	33.2	-.0247	-.0517	-.0012	-.0776	.0270	-.1070	.0553	-.1399	.0858	-.1634	.1187
	57.0	-.0306	-.0635	-.0094	-.0752	.0141	-.0929	.0376	-.1317	.0647	-.1693	.0941
	72.0	-.0306	-.0553	-.0129	-.0694	.0106	-.0764	.0329	-.0788	.0600	-.1023	.0870
	84.9	-.0447	-.0576	-.0188	-.0752	.0035	-.0811	.0247	-.0905	.0506	-.0988	.0776
	92.4	-.0553	-.0741	-.0364	-.0858	-.0153	-.0929	.0141	-.1011	.0259	-.1093	.0506
0.555	7.0	0.0047	-0.0410	0.0410	-0.0855	0.0820	-0.1335	0.1183	-0.1698	0.1534	-0.1909	0.1874
	14.1	-.0281	-.0703	.0059	-.1089	.0457	-.1452	.0820	-.1721	.1183	-.1838	.1534
	27.6	-.0457	-.0796	-.0164	-.1089	.0187	-.1382	.0527	-.1686	.0855	-.1827	.1194
	42.1	-.0504	-.0867	-.0269	-.1089	.0047	-.1429	.0363	-.1710	.0667	-.1862	.0995
	66.3	-.0527	-.0831	-.0340	-.1148	-.0059	-.1511	.0211	-.1780	.0492	-.1909	.0785
	77.3	-.0539	-.0796	-.0351	-.1171	-.0105	-.1546	.0152	-.1792	.0433	-.1909	.0726
	88.8	-.0691	-.0890	-.0492	-.1183	-.0269	-.1581	-.0012	-.1827	.0222	-.1967	.0480
0.777	11.6	-0.0246	-0.0785	0.0176	-0.1206	0.0609	-0.1663	0.0995	-0.1920	0.1347	-0.2049	0.1686
	22.3	-.0632	-.1077	-.0234	-.1417	.0199	-.1745	.0574	-.1920	.0925	-.2002	.1288
	33.6	-.0785	-.1206	-.0433	-.1452	-.0012	-.1686	.0340	-.1850	.0679	-.1932	.1030
	56.3	-.0843	-.1194	-.0574	-.1393	-.0234	-.1616	.0094	-.1792	.0386	-.1909	.0679
	79.4	-.0925	-.1183	-.0667	-.1370	-.0363	-.1593	-.0094	-.1792	.0164	-.1909	.0433

$R = 3.90 \times 10^6$

$\alpha = 0°$	$\alpha = 2°$		$\alpha = 4°$		$\alpha = 6°$		$\alpha = 8°$		$\alpha = 10°$	
C_p	C_{p_u}	C_{p_l}	C_{p_u}	C_{p_l}	C_{p_u}	C_{p_l}	C_{p_u}	C_{p_l}	C_{p_u}	C_{p_l}
0.0347	0.0049	0.0654	-0.0262	0.0974	-0.0587	0.1315	-0.1123	0.1662	-0.1458	0.2052
.0201	-.0067	.0478	-.0323	.0794	-.0539	.1132	-.0953	.1461	-.1355	.1851
.0049	-.0234	.0286	-.0435	.0557	-.0658	.0864	-.0709	.1184	-.1029	.1592
-.0082	-.0289	.0146	-.0508	.0414	-.0667	.0718	-.0816	.1038	-.0989	.1400
-.0073	-.0259	.0152	-.0408	.0414	-.0627	.0715	-.0779	.1035	-.0874	.1406
-.0195	-.0362	.0003	-.0545	.0240	-.0679	.0517	-.0819	.0828	-.0916	.1172
-.0155	-.0320	.0043	-.0511	.0271	-.0654	.0548	-.0791	.0846	-.0889	.1190
-.0195	-.0402	-.0003	-.0527	.0216	-.0676	.0478	-.0804	.0758	-.0910	.1090
-.0310	-.0490	-.0131	-.0633	.0073	-.0743	.0295	-.0834	.0548	-.0971	.0843
-.0463	-.0587	-.0259	-.0712	-.0085	-.0810	.0128	-.0941	.0359	-.1014	.0627
0.0180	-.0210	0.0566	-.0645	0.0922	-.1193	0.1297	-.1635	0.1635	-.1881	0.1979
-.0225	-.0575	.0116	-.0883	.0432	-.1196	.0782	-.1571	.1123	-.1811	.1540
-.0280	-.0563	-.0012	-.0898	.0292	-.1242	.0624	-.1632	.0947	-.1848	.1333
-.0216	-.0460	.0055	-.0740	.0356	-.1099	.0664	-.1644	.0998	-.1775	.1385
-.0323	-.0530	-.0097	-.0651	.0140	-.0858	.0426	-.0971	.0697	-.1702	.1050
-.0338	-.0563	-.0135	-.0712	.0061	-.0849	.0323	-.0925	.0600	-.1333	.0916
-.0417	-.0595	-.0204	-.0724	.0012	-.0861	.0253	-.0947	.0508	-.1001	.0816
-.0581	-.0724	-.0387	-.0840	-.0207	-.0965	.0003	-.1032	.0225	-.1087	.0505
0.0012	-.0491	0.0451	-.0927	0.0869	-.1473	0.1263	-.1751	0.1638	-.1995	0.2004
-.0348	-.0793	.0067	-.1223	.0482	-.1586	.0885	-.1751	.1275	-.1922	.1656
-.0473	-.0936	-.0131	-.1369	.0235	-.1668	.0601	-.1729	.0964	-.1937	.1345
-.0534	-.0845	-.0250	-.1318	.0058	-.1665	.0375	-.1800	.0720	-.1989	.1049
-.0540	-.0807	-.0296	-.0985	-.0021	-.1388	.0244	-.1821	.0552	-.1940	.0881
-.0540	-.0756	-.0302	-.0924	-.0064	-.1220	.0214	-.1754	.0500	-.1937	.0811
-.0644	-.0802	-.0442	-.0991	-.0232	-.1208	.0009	-.1745	.0287	-.1979	.0561
-.0253	-.0805	0.0210	-.1336	0.0650	-.1806	0.1068	-.2010	0.1394	-.2074	0.1766
-.0641	-.1129	-.0195	-.1531	.0238	-.1909	.0653	-.1958	.1028	-.2059	.1409
-.0814	-.1281	-.0388	-.1610	.0024	-.1961	.0406	-.1952	.0790	-.2059	.1138
-.0906	-.1379	-.0509	-.1702	-.0207	-.1922	.0116	-.1952	.0433	-.2074	.0759
-.0878	-.1339	-.0586	-.1708	-.0314	-.1903	-.0040	-.1983	.0238	-.2101	.0515

NACA

TABLE I.- EXPERIMENTAL PRESSURE COEFFICIENTS - Continued

$R = 12.6 \times 10^6$																							
Station		$\alpha = 0^\circ$	$\alpha = 2^\circ$		$\alpha = 4^\circ$		$\alpha = 6^\circ$		$\alpha = 8^\circ$		$\alpha = 10^\circ$		$\alpha = 12^\circ$		$\alpha = 14^\circ$		$\alpha = 16^\circ$		$\alpha = 18^\circ$		$\alpha = 20^\circ$	
$\frac{y}{b/2}$	Percent c	c_p	c_{p_u}	c_{p_l}	c_{p_u}	c_{p_l}	c_{p_u}	c_{p_l}	c_{p_u}	c_{p_l}	c_{p_u}	c_{p_l}	c_{p_u}	c_{p_l}	c_{p_u}	c_{p_l}	c_{p_u}	c_{p_l}	c_{p_u}	c_{p_l}	c_{p_u}	c_{p_l}
0.111	0	0.2216	0.2128	0.2251	0.1897	0.2161	0.1685	0.1970	0.1534	0.1688	0.1270	0.1430	0.1068	0.1135	0.1020	0.0820	0.0860	0.0499	0.0800	0.0254	0.0852	-0.0033
	3.8	.0620	.0369	.0960	.0007	.1362	-.0338	.1735	-.0625	.2067	-.1272	.2408	-.1456	.2941	-.1637	.3256	-.1786	.3826	-.1875	.4252	-.1811	.4807
	7.3	.0345	.0131	.0849	-.0246	.1017	-.0475	.1104	-.0616	.1616	-.1016	.1829	-.1437	.2370	-.1619	.2762	-.1732	.3401	-.1838	.3814	-.1872	.4431
	10.6	.0168	-.0162	.0424	-.0372	.0654	-.0520	.1032	-.0701	.1364	-.0943	.1798	-.1236	.2200	-.1472	.2588	-.1604	.3068	-.1838	.3513	-.1903	.4036
	14.2	.0052	-.0199	.0258	-.0444	.0636	-.0611	.0960	-.0766	.1111	-.0961	.1602	-.1218	.2102	-.1490	.2450	-.1658	.3050	-.1897	.3549	-.1903	.4063
	17.5	.0070	-.0144	.0332	-.0399	.0600	-.0557	.0924	-.0672	.1219	-.0888	.1402	-.1163	.1780	-.1490	.2331	-.1695	.2883	-.1930	.3348	-.2038	.3879
	21.2	.0052	-.0153	.0295	-.0381	.0527	-.0529	.0798	-.0654	.1039	-.0891	.1393	-.1071	.1796	-.1436	.2148	-.1713	.2643	-.1985	.3102	-.2087	.3613
	24.7	.0053	-.0144	.0314	-.0364	.0491	-.0502	.0744	-.0635	.1039	-.0833	.1348	-.0999	.1780	-.1307	.2111	-.1677	.2606	-.1948	.3065	-.2040	.3567
	28.2	.0062	-.0153	.0221	-.0363	.0454	-.0502	.0708	-.0597	.0985	-.0815	.1294	-.0925	.1706	-.1069	.2057	-.1458	.2514	-.1802	.2938	-.1888	.3476
	31.7	-.0040	-.0199	.0148	-.0417	.0400	-.0538	.0654	-.0654	.0895	-.0833	.1221	-.0925	.1652	-.0959	.1956	-.1257	.2440	-.1655	.2910	-.1750	.3439
	38.2	-.0095	-.0251	.0074	-.0489	.0291	-.0611	.0564	-.0710	.0804	-.0888	.1139	-.0962	.1541	-.1014	.1828	-.1147	.2292	-.1472	.2746	-.1682	.3218
	43.7	-.0132	-.0327	.0074	-.0525	.0255	-.0611	.0492	-.0710	.0732	-.0888	.1040	-.0962	.1467	-.1032	.1773	-.1129	.2255	-.1380	.2691	-.1573	.3182
	49.2	-.0169	-.0346	.0018	-.0507	.0218	-.0647	.0456	-.0710	.0714	-.0906	.1031	-.0999	.1412	-.1069	.1736	-.1166	.2209	-.1380	.2636	-.1508	.3126
	55.0	-.0169	-.0346	0	-.0543	.0218	-.0657	.0456	-.0710	.0714	-.0906	.1022	-.0999	.1402	-.1069	.1718	-.1184	.2181	-.1380	.2627	-.1508	.3108
	60.7	-.0169	-.0354	0	-.0543	.0218	-.0647	.0456	-.0729	.0714	-.0906	.1013	-.0999	.1412	-.1069	.1718	-.1166	.2200	-.1380	.2627	-.1493	.3108
	71.7	-.0205	-.0419	-.0055	-.0597	.0146	-.0702	.0365	-.0757	.0606	-.0943	.0877	-.0832	.1255	-.1105	.1562	-.1220	.1996	-.1399	.2371	-.1500	.2888
	77.5	-.0242	-.0437	-.0074	-.0615	.0109	-.0739	.0311	-.0804	.0534	-.0961	.0922	-.0889	.1338	-.1142	.1599	-.1267	.2084	-.1417	.2408	-.1493	.2878
	83.2	-.0225	-.0364	-.0097	-.0615	.0128	-.0748	.0329	-.0794	.0552	-.0980	.0849	-.0907	.1181	-.1160	.1507	-.1275	.2052	-.1417	.2508	-.1408	.2933
	88.7	-.0318	-.0492	-.0221	-.0642	-.0036	-.0757	.0347	-.0804	.0389	-.0980	.0732	-.1090	.1071	-.1179	.1388	-.1293	.1784	-.1435	.2161	-.1752	.2612
	94.0	-.0352	-.0620	-.0258	-.0759	-.0072	-.0830	.0275	-.0841	.0353	-.0998	.0550	-.1108	.0886	-.1197	.1132	-.1293	.1507	-.1417	.1878	-.1752	.2262
0.333	0	.1890	.1537	.1846	.1042	.1874	.0544	.1658	.0119	.1367	-.0166	.1130	-.0277	.0882	-.0531	.0724	-.0764	.0431	-.0922	.0216	-.1046	.0184
	4.8	.0401	-.0052	.0910	-.0615	.1254	-.0997	.1640	-.1308	.2002	-.1643	.2340	-.1802	.2701	-.1965	.3144	-.1967	.3451	-.1737	.3776	-.1790	.4265
	9.2	.0043	-.0335	.0464	-.0797	.0853	-.1251	.1222	-.1525	.1612	-.1815	.2015	-.1911	.2391	-.1956	.2851	-.1976	.3231	-.1792	.3648	-.1826	.4227
	14.2	-.0049	-.0481	.0258	-.0870	.0998	-.1287	.0950	-.1616	.1367	-.1896	.1689	-.1984	.2158	-.1975	.2631	-.1974	.3021	-.1855	.3448	-.1899	.4058
	18.7	-.0131	-.0445	.0202	-.0888	.0543	-.1124	.0876	-.1616	.1249	-.1914	.1599	-.1893	.2046	-.1956	.2502	-.2012	.2882	-.1882	.3320	-.1917	.3926
	23.2	-.0113	-.0426	.0193	-.0779	.0525	-.1114	.0860	-.1390	.1222	-.1608	.1527	-.1757	.1946	-.1928	.2411	-.1985	.2801	-.1901	.3266	-.1935	.3832
	28.2	-.0177	-.0445	.0100	-.0743	.0379	-.1006	.0696	-.1290	.1040	-.1545	.1365	-.1747	.1764	-.1947	.2200	-.2021	.2563	-.1991	.2993	-.2017	.3587
	32.7	-.0178	-.0417	.0045	-.0706	.0352	-.0933	.0641	-.1227	.0967	-.1536	.1274	-.1747	.1664	-.1947	.2099	-.2021	.2472	-.1955	.2920	-.1989	.3484
	40.2	-.0232	-.0445	-.0050	-.0706	.0215	-.0897	.0478	-.1146	.0786	-.1572	.1076	-.1739	.1448	-.1910	.1860	-.1976	.2234	-.1756	.2638	-.1868	.3213
	47.5	-.0324	-.0499	-.0095	-.0724	.0151	-.0897	.0406	-.1137	.0722	-.1644	.1022	-.1847	.1391	-.2012	.1806	-.2048	.2225	-.1919	.2628	-.1953	.3202
	55.0	-.0324	-.0499	-.0095	-.0733	.0160	-.0888	.0369	-.1083	.0659	-.1608	.0949	-.1902	.1318	-.2049	.1714	-.2093	.2096	-.1955	.2501	-.1989	.3042
	62.7	-.0340	-.0545	-.0188	-.0761	.0051	-.0897	.0297	-.1010	.0577	-.1464	.0868	-.1902	.1245	-.2086	.1595	-.2120	.1904	-.1901	.2359	-.1935	.2891
	70.2	-.0397	-.0573	-.0198	-.0779	-.0004	-.0906	.0215	-.0992	.0505	-.1166	.0769	-.1865	.1127	-.2128	.1558	-.2147	.1824	-.1955	.2246	-.1989	.2873
	77.5	-.0434	-.0609	-.0243	-.0779	-.0004	-.0897	.0279	-.0956	.0659	-.0929	.0877	-.1602	.1136	-.2067	.1476	-.2129	.1767	-.1973	.2100	-.2006	.2778
	85.0	-.0379	-.0627	-.0206	-.0815	-.0023	-.0942	.0133	-.0992	.0362	-.1049	.0513	-.1275	.0901	-.1919	.1374	-.2018	.1758	-.1846	.2119	-.1890	.2628
	92.5	-.0544	-.0673	-.0448	-.0815	-.0259	-.0924	.0103	-.1028	.0251	-.1121	.0498	-.1212	.0826	-.1752	.1145	-.1976	.1447	-.1828	.1855	-.1871	.2345
0.555	0	.1933	.1729	.1744	.1260	.1455	.0817	.0896	.0480	.0414	.0190	-.0008	-.0011	-.0283	-.0291	-.0422	-.0432	-.0612	-.0614	-.0768	-.0728	-.0928
	7.5	.0135	-.0335	.0630	-.0815	.1145	-.1178	.1566	-.1588	.1966	-.1878	.2277	-.2029	.2683	-.2086	.3061	-.2075	.3387	-.1955	.3703	-.1980	.4161
	14.2	-.0204	-.0755	.0221	-.1180	.0689	-.1477	.1077	-.1733	.1512	-.1978	.1879	-.2066	.2318	-.2067	.2741	-.2075	.3121	-.1937	.3512	-.1962	.4039
	21.2	-.0416	-.0819	.0007	-.1344	.0416	-.1623	.0760	-.1796	.1185	-.2029	.1527	-.2066	.1937	-.2076	.2374	-.2084	.2783	-.1919	.3220	-.1953	.3795
	28.7	-.0495	-.0765	-.0099	-.1344	.0373	-.1636	.0633	-.1841	.1040	-.2058	.1365	-.2074	.1755	-.2086	.2190	-.2102	.2545	-.1955	.3029	-.1971	.3569
	35.2	-.0434	-.0746	-.0132	-.1307	.0273	-.1649	.0487	-.1814	.0859	-.2029	.1148	-.2002	.1573	-.2049	.2025	-.2066	.2393	-.1882	.2811	-.1926	.3380
	42.2	-.0471	-.0701	-.0169	-.1180	.0218	-.1659	.0451	-.1850	.0804	-.1978	.1112	-.1974	.1491	-.2067	.1897	-.2093	.2206	-.1937	.2710	-.1971	.3362
	50.0	-.0544	-.0709	-.0318	-.1070	-.0031	-.1387	.0279	-.1579	.0614	-.1779	.0940	-.1974	.1300	-.2076	.1695	-.2120	.2060	-.1991	.2483	-.2017	.3305
	57.5	-.0526	-.0673	-.0321	-.0979	-.0068	-.1278	.0242	-.1507	.0577	-.1743	.0769	-.1884	.1054	-.2012	.1384	-.2090	.1690	-.1774	.2058	-.1817	.2741
	65.0	-.0654	-.0765	-.0347	-.1016	-.0150	-.1332	.0006	-.1642	.0242	-.1851	.0426	-.1992	.0893	-.2123	.1219	-.2129	.1538	-.1955	.1973	-.1953	.2515
0.777	0	.1537	.1309	.1384	.0736	.0908	.0099	.0492	-.0340	.0191	-.0723	-.0030	-.1017	-.0210	-.1197	-.0407	-.1384	-.0610	-.1545	-.0705	-.1873	-.0843
	10.0	-.0334	-.0895	.0185	-.1317	.0636	-.1596	.1104	-.1696	.1454	-.2058	.1810	-.1986	.2232	-.2095	.2505	-.2151	.2928	-.2187	.3202	-.2330	.3494
	23.7	-.0590	-.1151	-.0721	-.1551	.0327	-.1796	.0726	-.1743	.1111	-.2095	.1520	-.1968	.1973	-.2095	.2295	-.2151	.2662	-.2187	.3038	-.2330	.3650
	35.7	-.0572	-.1188	-.0240	-.1588	.0128	-.1750	.0492	-.1508	.0858	-.2089	.1221	-.1803	.1660	-.1985	.1974	-.2060	.2589	-.2132	.2936	-.2271	.3318
	47.7	-.0609	-.1243	-.0332	-.1642	.0001	-.1778	.0293	-.1536	.0660	-.2003	.1022	-.1821	.1541	-.1985	.1956	-.2078	.2273	-.2132	.2545	-.2278	.2864
	71.7	-.0737	-.1262	-.0443	-.1677	-.0072	-.1860	.0275	-.1780	.0678	-.2191	.0949	-.2004	.1273	-.2113	.1590	-.2206	.2218	-.2168	.2572	-.2330	.2888
	83.7	-.0700	-.1262	-.0461	-.1669	-.0127	-.1850	.0221	-.1667	.0462	-.2077	.0786	-.1913	.1060	-.2077	.1635	-.2133	.1995	-.2150	.2271	-.2306	.2573

TABLE I.- EXPERIMENTAL PRESSURE COEFFICIENTS - Concluded

R = 18.3 × 10⁶																			
Station		α = 0°	α = 2°		α = 4°		α = 6°		α = 8°		α = 10°		α = 12°		α = 14°		α = 16°	
$\frac{y}{b/2}$	Percent c	c_p	c_{p_u}	c_{p_l}	c_{p_u}	c_{p_l}	c_{p_u}	c_{p_l}	c_{p_u}	c_{p_l}	c_{p_u}	c_{p_l}	c_{p_u}	c_{p_l}	c_{p_u}	c_{p_l}	c_{p_u}	c_{p_l}
0.111	0	0.2250	0.2075	0.2140	0.1911	0.1965	0.1642	0.1841	0.1421	0.1706	0.1241	0.1490	0.1071	0.1039	0.0997	0.0805	0.1001	0.0448
	3.8	.0648	.0308	.0966	.0027	.1374	-.0362	.1727	-.0797	.2033	-.1258	.2438	-.1372	.2873	-.1550	.3333	-.1651	.3732
	7.3	.0423	.0081	.0617	-.0262	.0922	-.0512	.1397	-.0772	.1631	-.1057	.1844	-.1334	.2336	-.1580	.2853	-.1657	.3232
	10.6	.0122	-.0171	.0417	-.0350	.0721	-.0550	.1034	-.0809	.1404	-.0969	.1806	-.1295	.2137	-.1463	.2600	-.1670	.2976
	14.2	.0066	-.0196	.0180	-.0419	.0633	-.0613	.0934	-.0822	.1266	-.0981	.1667	-.1198	.2022	-.1597	.2511	-.1772	.2972
	17.5	.0097	-.0139	.0279	-.0381	.0445	-.0556	.0908	-.0747	.1241	-.0912	.1478	-.1135	.1925	-.1537	.2385	-.1823	.2797
	21.2	.0035	-.0158	.0336	-.0962	.0487	-.0538	.0770	-.0722	.1065	-.0834	.1427	-.1048	.1762	-.1537	.2221	-.1886	.2634
	24.7	.0010	-.0139	.0192	-.0331	.0364	-.0519	.0877	-.0697	.1052	-.0855	.1369	-.0948	.1750	-.1588	.2195	-.1810	.2596
	28.2	.0010	-.0177	.0180	-.0356	.0294	-.0519	.0669	-.0697	.0990	-.0836	.1351	-.0886	.1750	-.1206	.2246	-.1479	.2521
	31.7	-.0034	-.0202	.0142	-.0375	.0370	-.0569	.0691	-.0722	.0964	-.0855	.1326	-.0913	.1600	-.0941	.2031	-.1263	.2433
	38.2	-.0109	-.0278	.0067	-.0463	.0295	-.0625	.0555	-.0772	.0851	-.0881	.1187	-.0961	.1476	-.1040	.1905	-.1212	.2258
	43.7	-.0153	-.0329	.0017	-.0501	.0244	-.0644	.0505	-.0797	.0776	-.0906	.1124	-.0986	.1438	-.1065	.1854	-.1187	.2245
	49.2	-.0178	-.0354	-.0014	-.0488	.0229	-.0669	.0467	-.0797	.0751	-.0906	.1086	-.0998	.1375	-.1090	.1791	-.1187	.2220
	55.0	-.0191	-.0354	-.0020	-.0513	.0207	-.0669	.0442	-.0809	.0726	-.0912	.1061	-.0998	.1388	-.1103	.1765	-.1199	.2145
	60.7	-.0184	-.0367	-.0020	-.0520	.0232	-.0663	.0455	-.0784	.0738	-.0906	.0997	-.1011	.1226	-.1090	.1766	-.1193	.2158
	71.7	-.0266	-.0429	.0101	-.0490	.0131	-.0732	.0354	-.0847	.0613	-.0956	.0922	-.1048	.1088	-.1127	.1601	-.1237	.1983
	77.5	-.0303	-.0449	-.0133	-.0601	.0094	-.0744	.0304	-.0872	.0537	-.0869	.0884	-.1073	.1076	-.1164	.1638	-.1269	.1995
	83.2	-.0353	-.0404	-.0133	-.0620	.0100	-.0769	.0354	-.0884	.0575	-.0994	.0898	-.1086	.1014	-.1164	.1563	-.1288	.1992
	88.7	-.0291	-.0505	-.0170	-.0633	.0056	-.0782	.0304	-.0897	.0599	-.0975	.0745	-.1086	.0964	-.1251	.1437	-.1298	.1820
	94.0	-.0441	-.0619	-.0308	-.0752	-.0180	-.0857	.0089	-.0935	.0366	-.0988	.0606	-.1110	.0702	-.1276	.1184	-.1288	.1507
0.339	0	.1799	.1603	.1865	.1111	.0810	.0598	.1662	.0118	.1347	-.0113	.1174	-.0278	.0908	-.0577	.0679	-.0753	.0439
	4.8	.0358	-.0082	.0799	-.0593	.1298	-.0971	.1606	-.2323	.1950	-.1636	.2346	-.1764	.2687	-.1987	.3022	-.1957	.3402
	9.2	.0012	-.0354	.0454	-.0770	.0860	-.1229	.1205	-.1523	.1592	-.1794	.2025	-.1866	.2373	-.2037	.2745	-.1971	.3201
	14.2	-.0063	-.0493	.0267	-.0846	.0608	-.1267	.0954	-.1624	.1334	-.1869	.1729	-.1942	.2134	-.2037	.2531	-.1995	.2986
	18.7	-.0151	-.0467	.0197	-.0865	.0545	-.1110	.0879	-.1617	.1234	-.1882	.1641	-.1866	.2034	-.2000	.2411	-.1995	.2860
	23.2	-.0120	-.0449	.0216	-.0758	.0539	-.1110	.0867	-.1411	.1190	-.1585	.1553	-.1714	.1939	-.1899	.2329	-.1995	.2784
	28.2	-.0189	-.0455	.0127	-.0796	.0406	-.1002	.0704	-.1310	.1039	-.1553	.1382	-.1733	.1757	-.1949	.2115	-.2032	.2545
	32.7	-.0214	-.0417	.0064	-.0676	.0368	-.0927	.0653	-.1248	.0969	-.1560	.1300	-.1733	.1663	-.1943	.2027	-.2032	.2457
	40.2	-.0271	-.0480	-.0037	-.0688	.0230	-.0889	.0478	-.1191	.0762	-.1610	.1086	-.1707	.1437	-.1880	.1775	-.1944	.2173
	47.5	-.0321	-.0518	-.0089	-.0662	.0167	-.0870	.0478	-.1154	.0731	-.1674	.1061	-.1841	.1387	-.1981	.1737	-.2070	.2198
	55.0	-.0327	-.0518	-.0089	-.0707	.0174	-.0870	.0403	-.1078	.0675	-.1642	.0985	-.1892	.1318	-.2006	.1668	-.2108	.2091
	62.7	-.0372	-.0550	-.0145	-.0733	.0860	-.0870	.0303	-.1003	.0592	-.1471	.0909	-.1873	.1261	-.2031	.1554	-.2121	.1889
	70.2	-.0397	-.0575	-.0139	-.0739	.0822	-.0876	.0221	-.0978	.0527	-.1048	.0809	-.1841	.1136	-.2062	.1517	-.2146	.2053
	77.5	-.0422	-.0606	-.0216	-.0745	.0009	-.0857	.0265	-.0953	.0649	-.0909	.0935	-.1536	.1186	-.2018	.1447	-.2133	.1770
	85.0	-.0365	-.0591	-.0178	-.0808	-.0010	-.0933	.0140	-.1016	.0335	-.1054	.0569	-.1250	.0859	-.1862	.1302	-.2007	.1713
	92.5	-.0992	-.0648	-.0431	-.0795	-.0262	-.0958	-.0117	-.1066	.0228	-.1130	.0506	-.1225	.0784	-.1717	.1044	-.1957	.1385
0.555	0	.1894	.1710	.1802	.1325	.1478	.0850	.0907	.0494	.0435	.0190	.0014	-.0084	-.0296	-.0270	-.0468	-.0437	-.0620
	7.5	.0119	-.0395	.0660	-.0770	.1144	-.1173	.1550	-.1992	.1931	-.1882	.2308	-.2000	.2655	-.2087	.2959	-.2083	.3352
	14.2	-.0233	-.0751	.0241	-.1162	.0581	-.1469	.1092	-.1730	.1498	-.1958	.1905	-.2025	.2304	-.2062	.2644	-.2076	.3087
	21.2	-.0428	-.0884	.0092	-.1339	.0406	-.1595	.0766	-.1793	.1164	-.2009	.1552	-.1993	.1921	-.2056	.2285	-.2064	.2747
	28.7	-.0435	-.0821	-.0092	-.1339	.0377	-.1632	.0664	-.1830	.1026	-.2034	.1388	-.2019	.1751	-.2056	.2127	-.2076	.2532
	35.2	-.0447	-.0808	-.0109	-.1307	.0192	-.1620	.0516	-.1805	.0838	-.2009	.1174	-.1917	.1556	-.2018	.1903	-.2045	.2343
	42.2	-.0466	-.0745	-.0146	-.1174	.0154	-.1632	.0478	-.1830	.0781	-.1888	.1136	-.1879	.1468	-.2043	.1819	-.2070	.2179
	49.0	-.0544	-.0758	-.0267	-.1042	-.0035	-.1368	.0278	-.1592	.0611	-.1794	.0960	-.1879	.1286	-.2056	.1624	-.2102	.2028
	77.5	-.0516	-.0739	-.0317	-.0985	-.0092	-.1261	.0171	-.1530	.0555	-.1756	.0777	-.1764	.1035	-.1956	.1302	-.1995	.1987
	88.7	-.0523	-.0821	-.0380	-.0998	-.0148	-.1305	.0027	-.1660	.0222	-.1882	.0693	-.1911	.0884	-.2061	.1164	-.2102	.1517
0.777	0	.1986	.1886	.1341	.0755	.0847	.0070	.0480	-.0421	.0198	-.0729	.0001	-.1036	-.0587	-.1269	-.0533	-.1390	-.0672
	10.0	-.0353	-.0894	.0142	-.1311	.0602	-.1609	.1085	-.1887	.1455	-.1970	.1819	-.1983	.1987	-.2059	.2499	-.2058	.2846
	23.7	-.0663	-.1142	-.0245	-.1531	.0295	-.1765	.0707	-.1824	.1128	-.1995	.1641	-.1971	.1775	-.2047	.2423	-.2042	.2996
	35.7	-.0779	-.1149	-.0332	-.1525	.0094	-.1684	.0492	-.1837	.0851	-.1856	.1250	-.2037	.1426	-.1860	.1968	-.1911	.2433
	47.7	-.0816	-.1212	-.0432	-.1569	-.0032	-.1721	.0322	-.1862	.0663	-.1869	.0947	-.2050	.1213	-.1873	.1841	-.1911	.2233
	71.7	-.0816	-.1250	-.0482	-.1650	-.0070	-.1834	.0272	-.1987	.0550	-.2014	.0997	-.1971	.1113	-.2059	.1664	-.2064	.2083
	83.7	-.0816	-.1237	-.0507	-.1632	-.0158	-.1797	.0076	-.1937	.0499	-.1945	.0833	-.1883	.0939	-.1972	.1551	-.2000	.1845

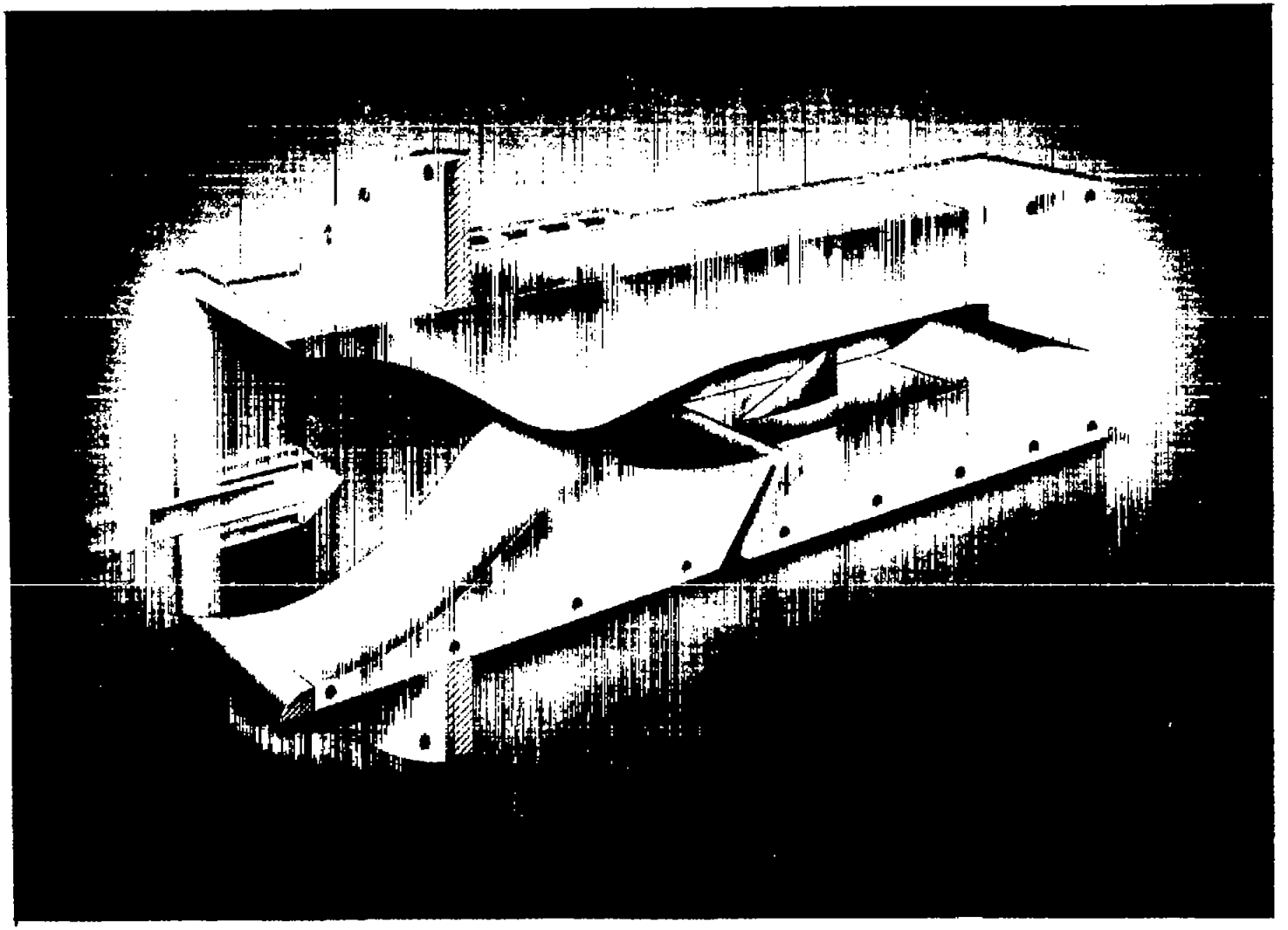

Figure 1.- M = 2.41 jet.

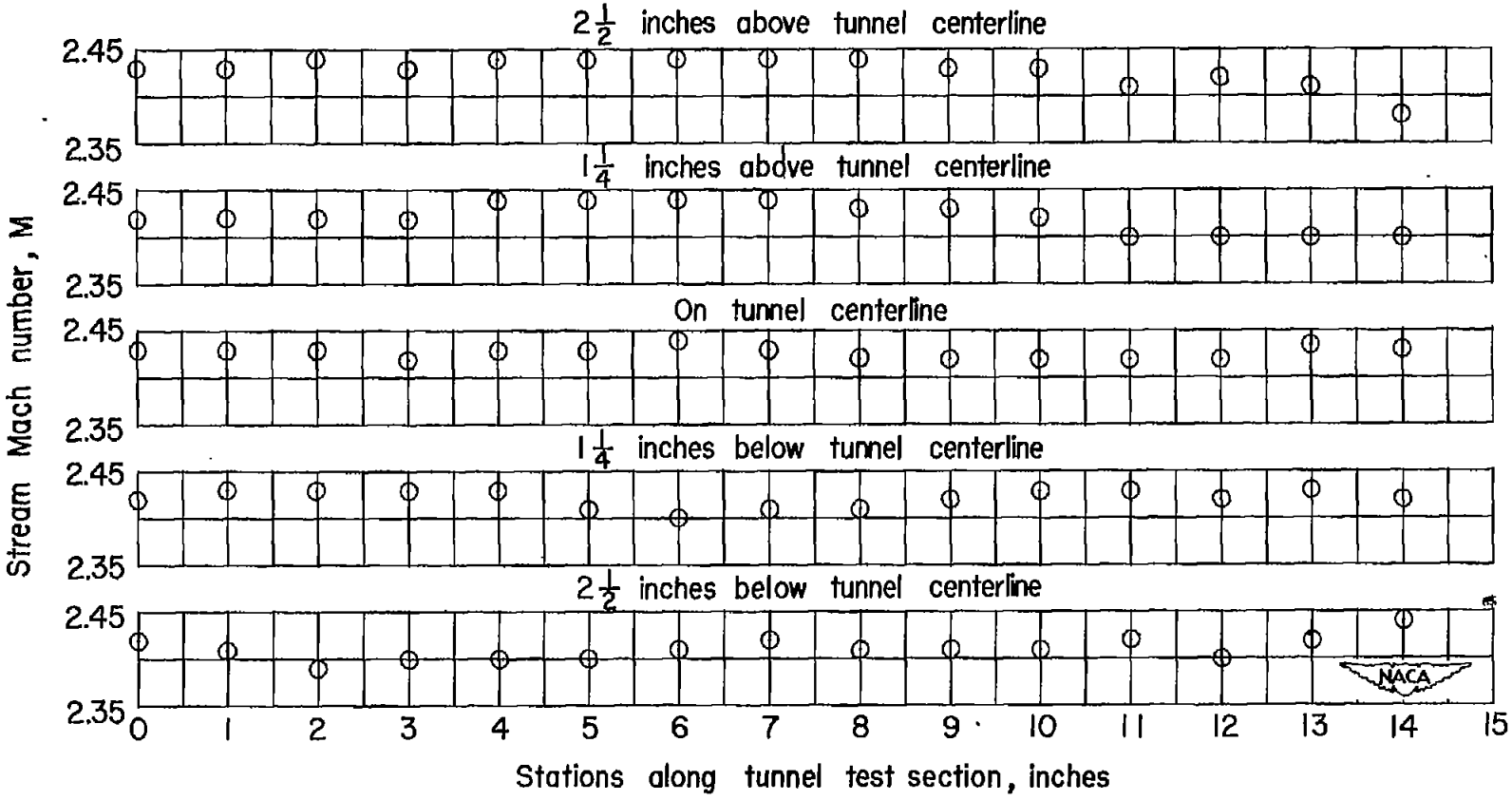

Figure 2.- Mach number distribution in the M = 2.41 blowdown jet test section.

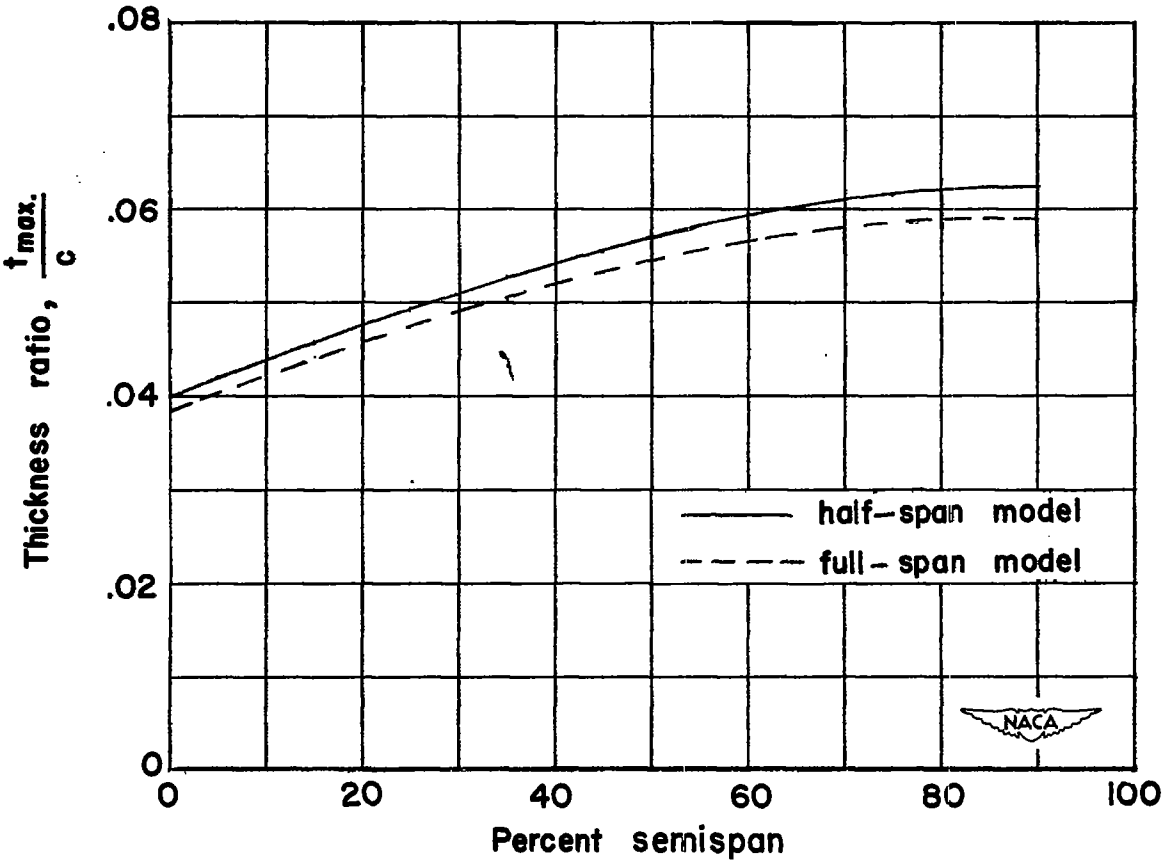

(a) Spanwise variation of thickness ratio.

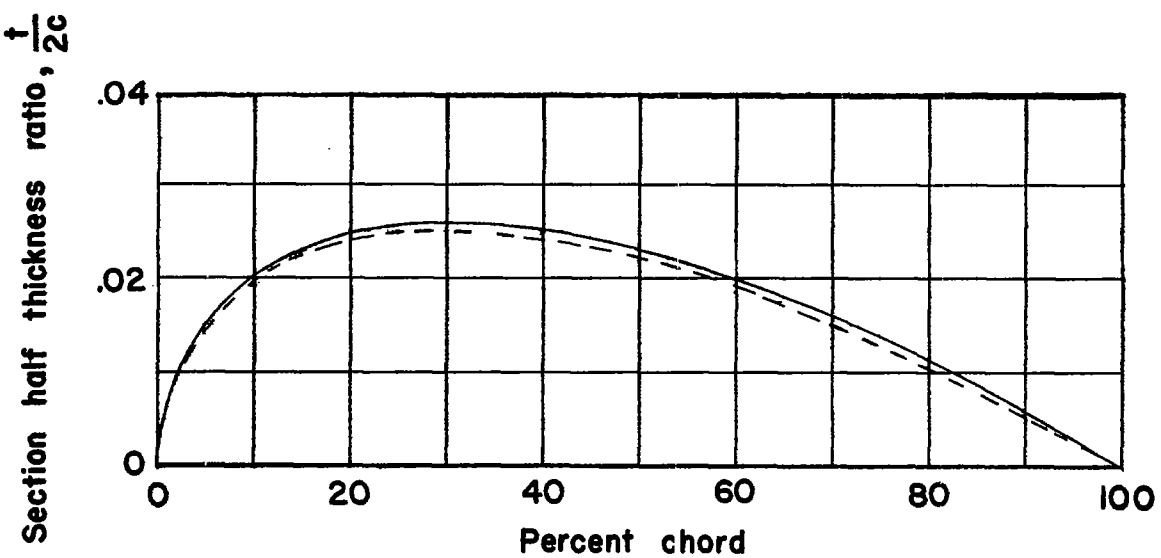

(b) Section shape at 0.333b/2.

Figure 3.- Wing-section properties.

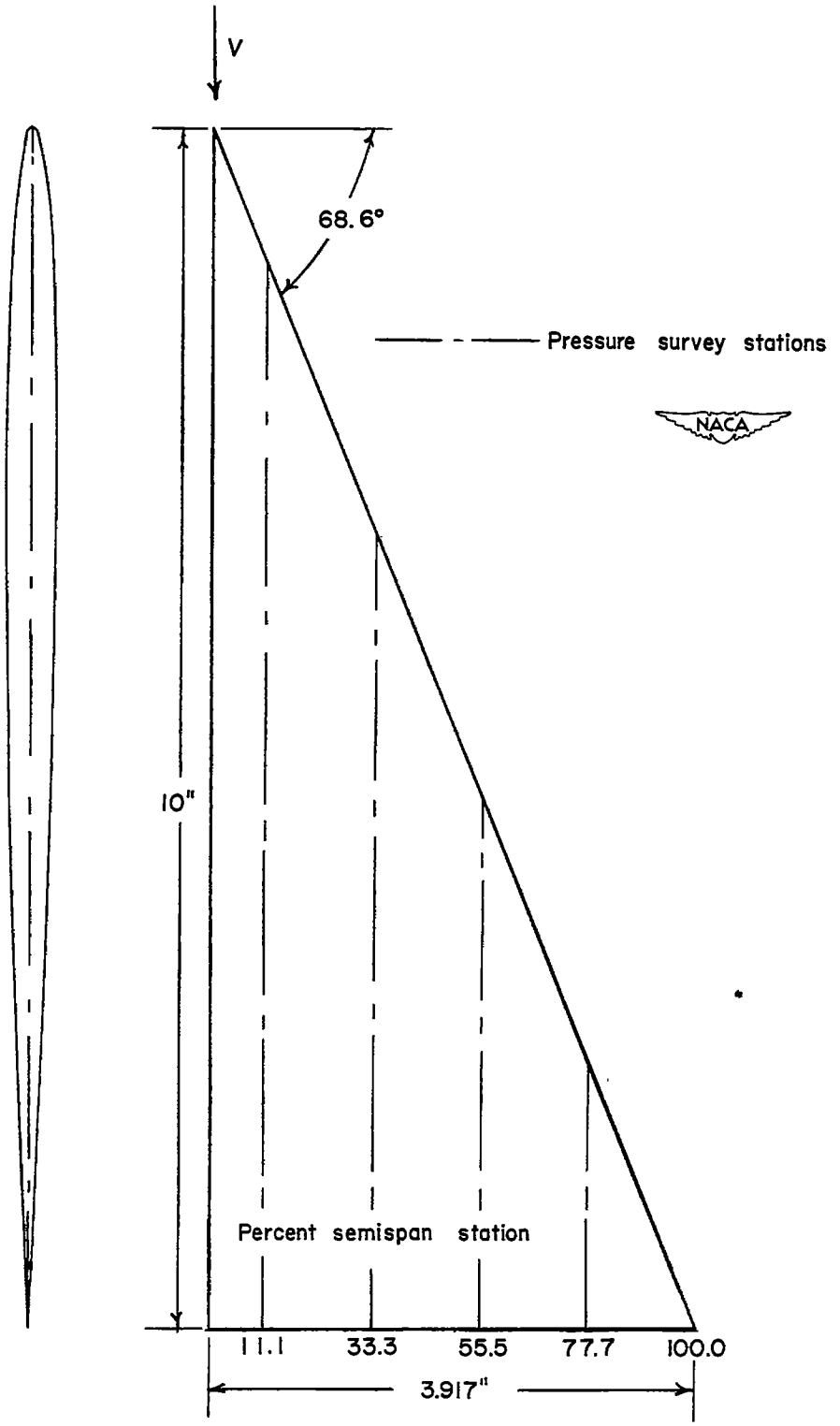

Figure 4.- Dimensional sketch of semispan triangular wing.

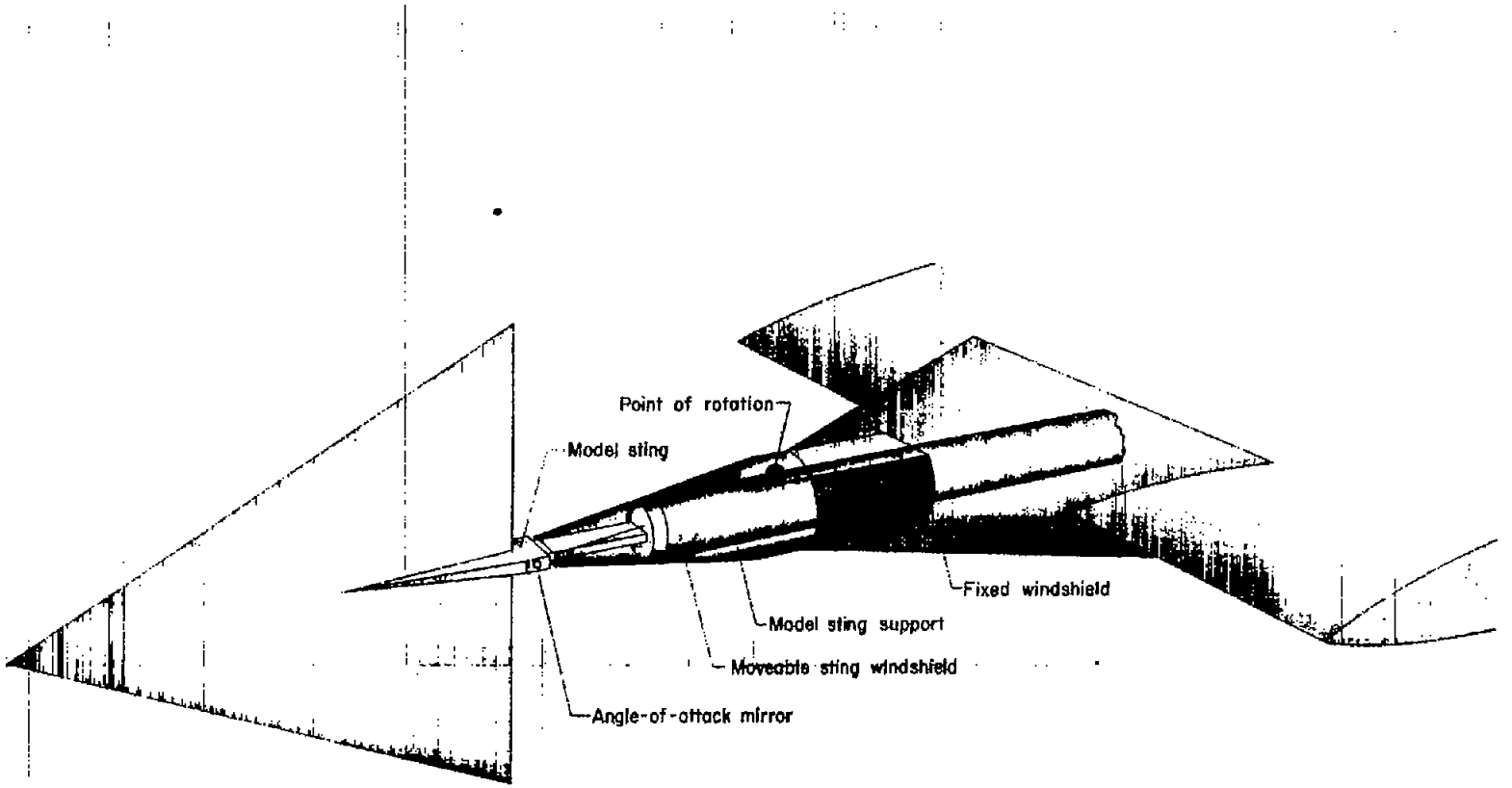

Figure 5.- Full-span wing mounted on sting.

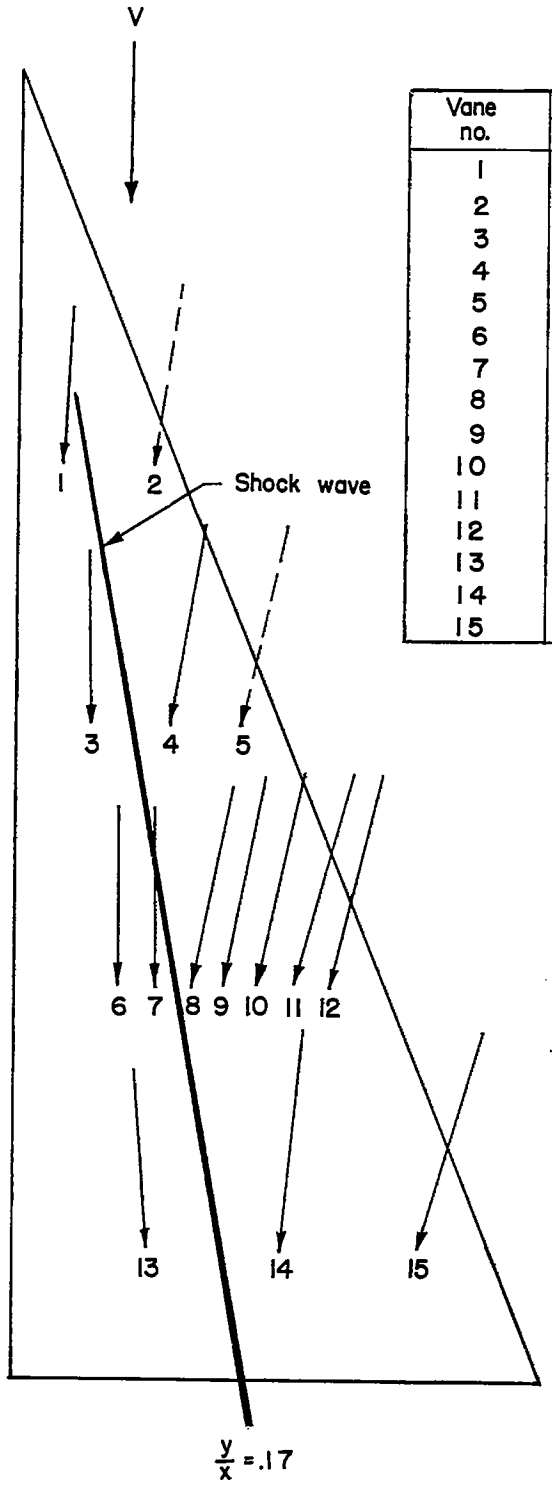

Vane no.	Vane location		Flow angle	Local Mach no.
	x/cr	y/cr		
1	.300	.035	3°36'	2.32
2	.300	.100	8°21'	—
3	.500	.055	− 0°45'	2.69
4	.500	.113	9°30'	3.09
5	.500	.170	11°39'	—
6	.700	.078	− 0°21'	2.75
7	.700	.105	0°33'	2.75
8	.700	.128	10°30'	3.14
9	.700	.158	9°57'	3.25
10	.700	.180	11°42'	3.31
11	.700	.208	14°00'	3.32
12	.700	.235	12°54'	3.35
13	.900	.100	− 4°24'	2.75
14	.900	.200	5°36'	3.34
15	.900	.300	15°18'	3.45

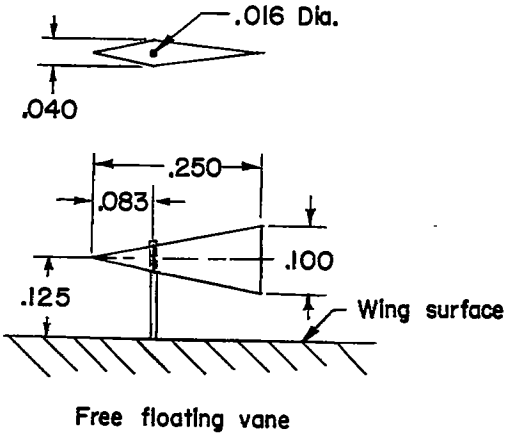

Free floating vane

Figure 6.- Local flow direction on wing upper surface as determined from vane survey. $\alpha = 10^{\circ}$; $R = 1.04 \times 10^{6}$.

[redacted]

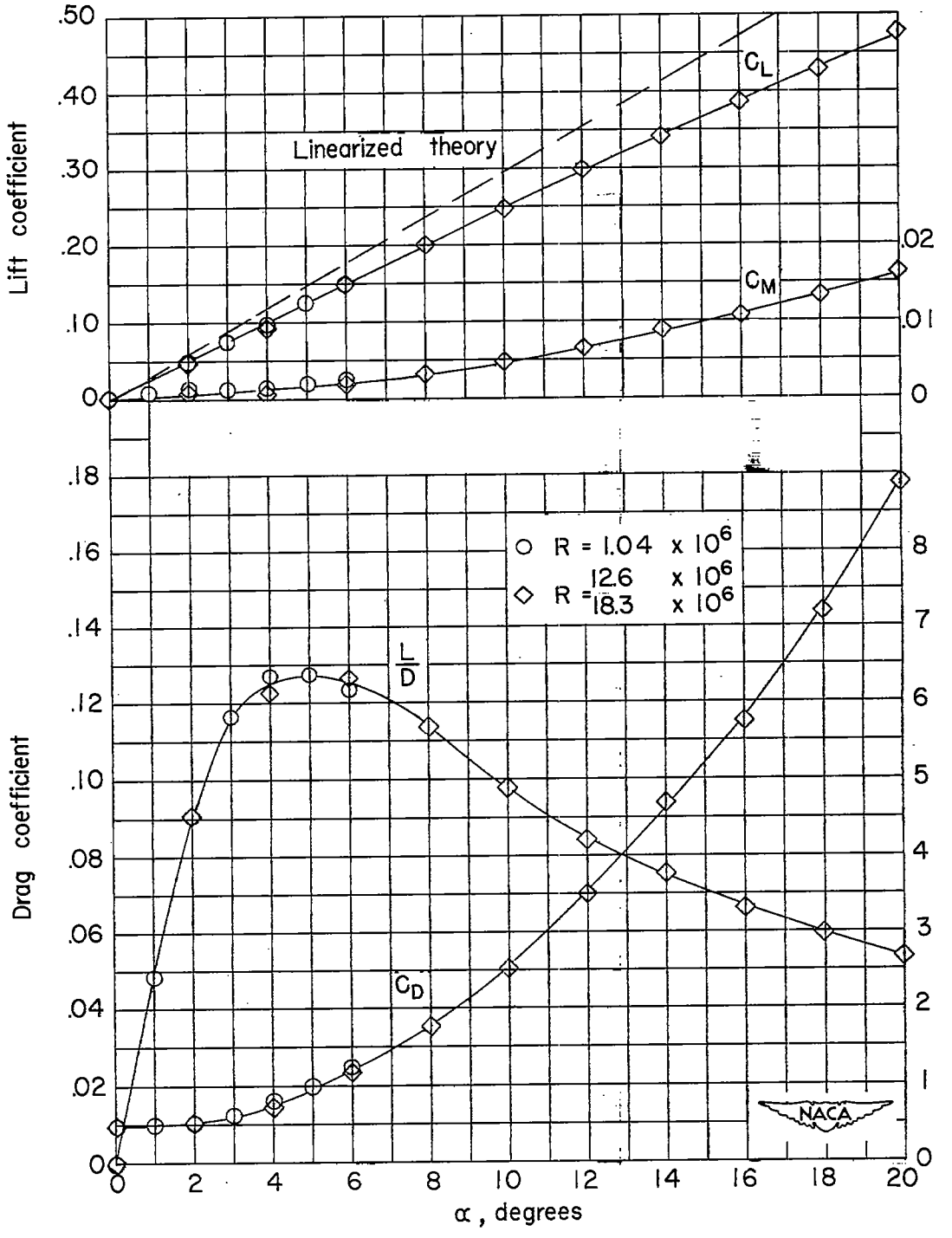

Figure 7.- Variation of wing aerodynamic characteristics with angle of attack for different Reynolds numbers.

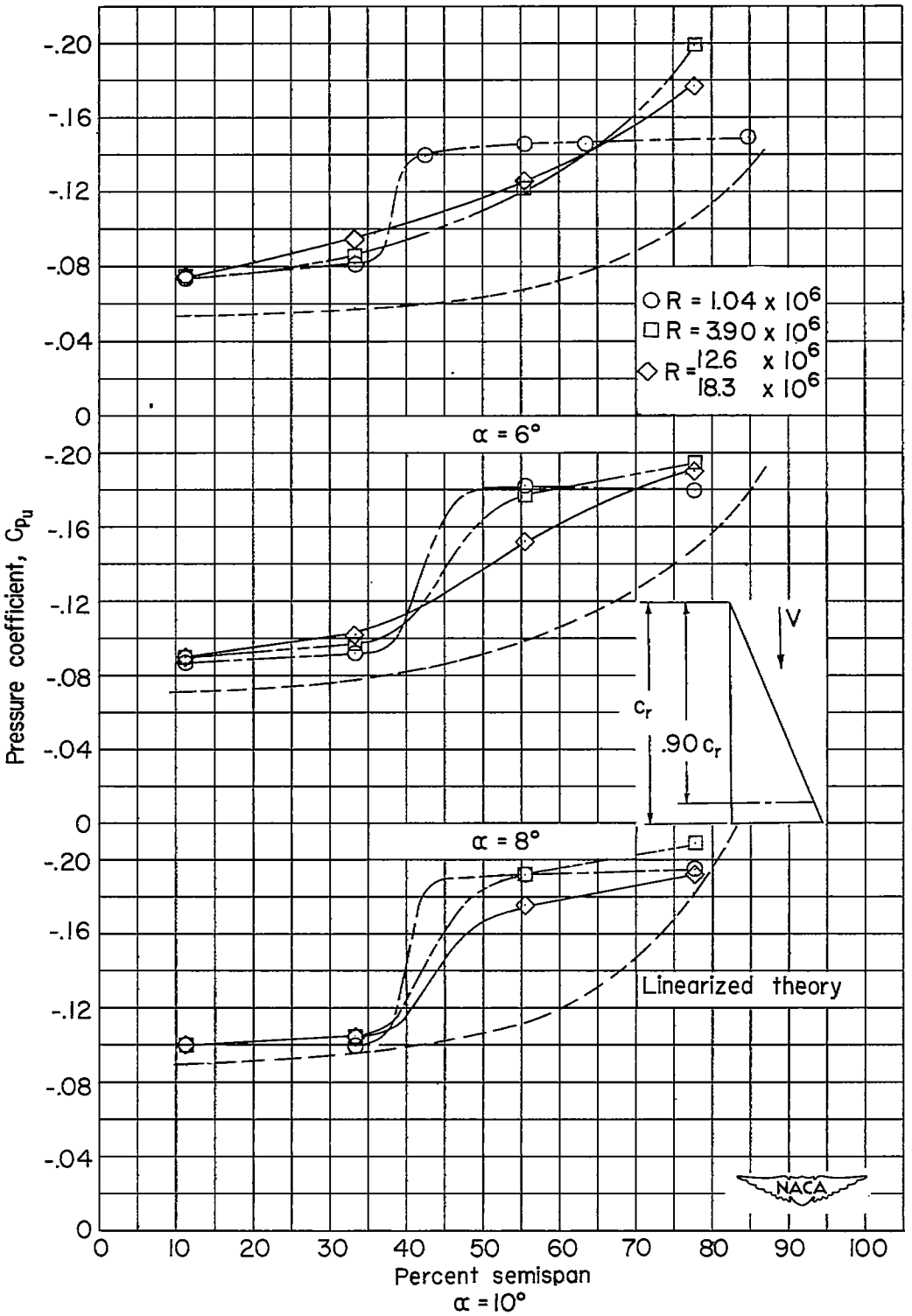

Figure 8.- Spanwise variation of upper-surface pressure coefficient at $0.90c_r$ at different Reynolds numbers.

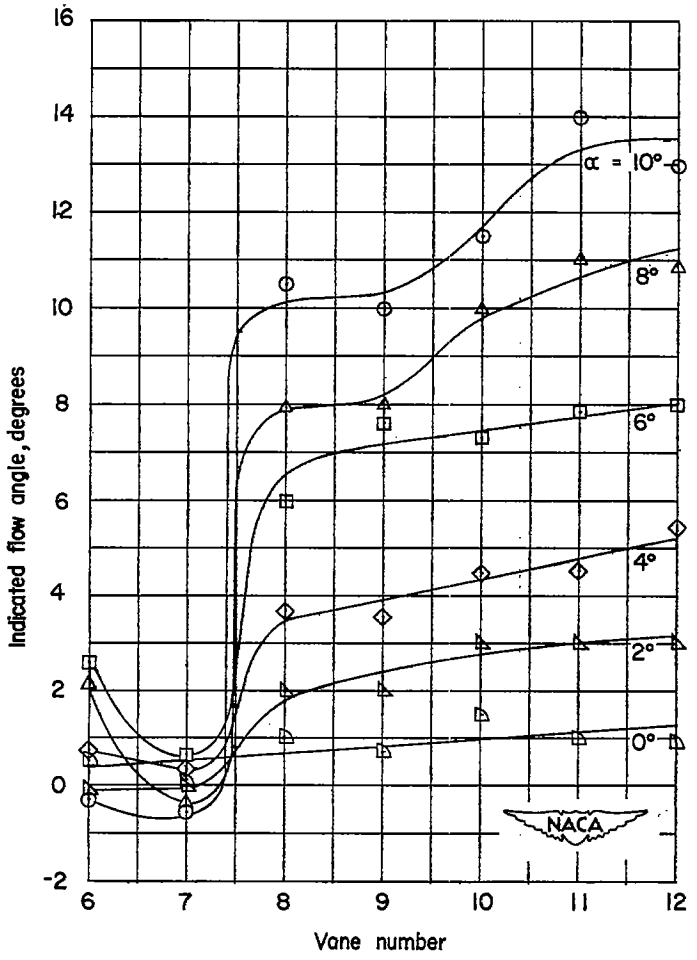

(a) Indicated flow angles.

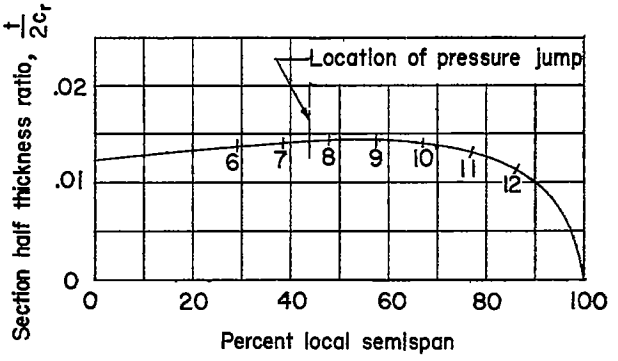

(b) Vane locations on wing profile.

Figure 9.- Results of vane survey on wing upper surface at $0.70c_r$ station. $R = 1.04 \times 10^6$.

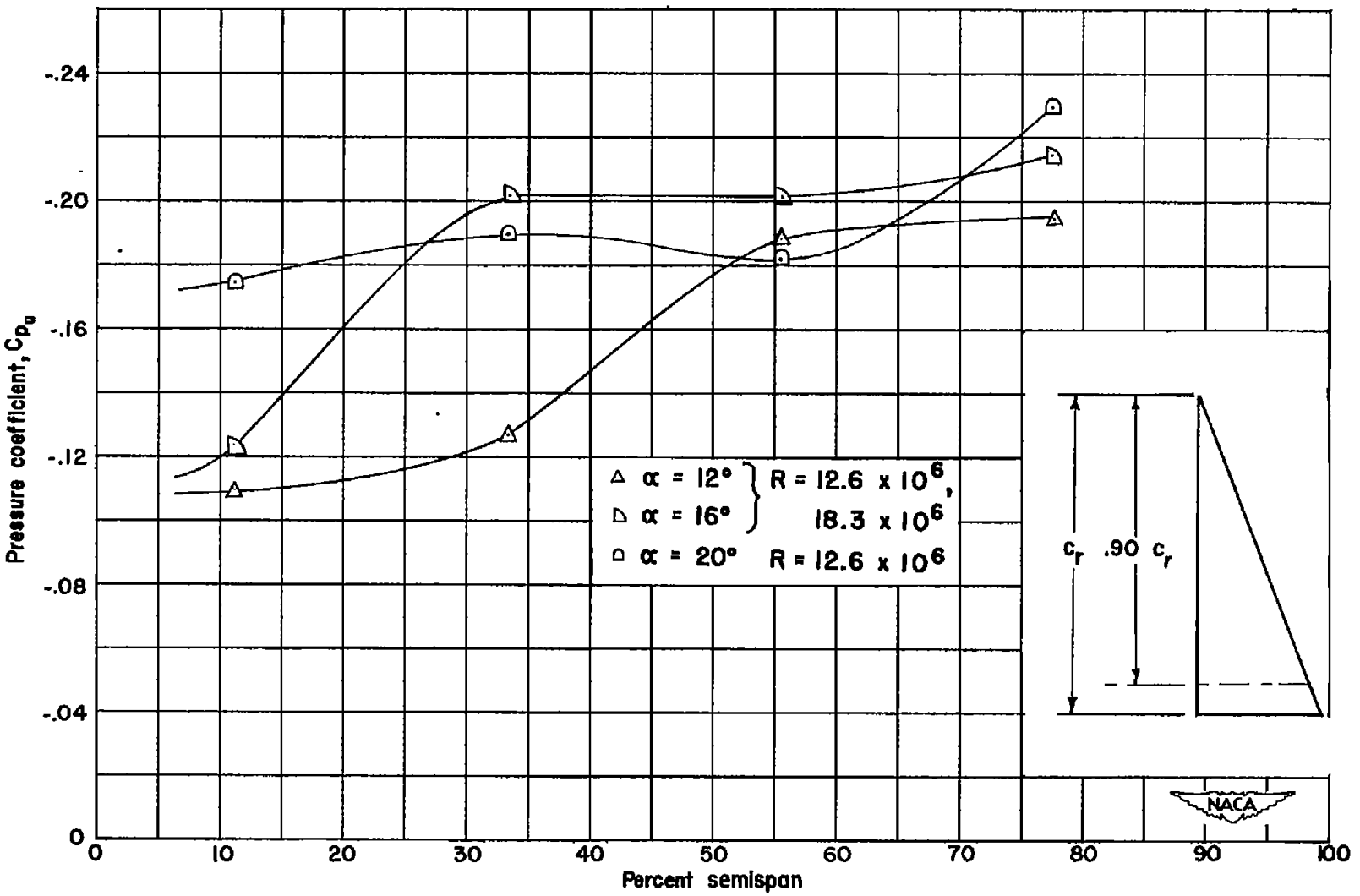

Figure 10.- Spanwise variation of upper-surface pressure coefficient at $0.90c_r$ at high angles of attack.

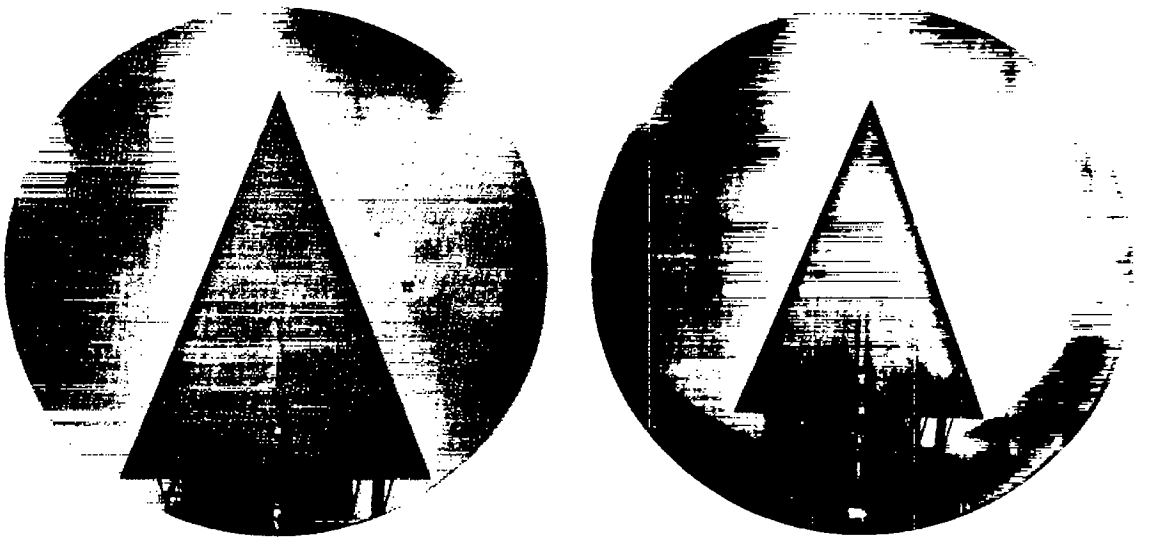

$\alpha = 0°$ $\alpha = 4°$

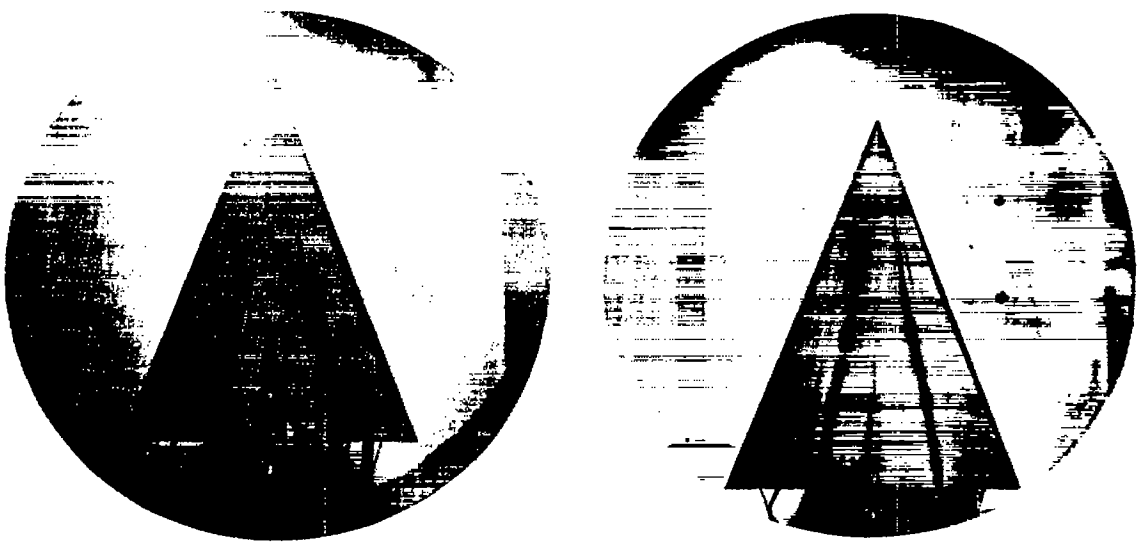

$\alpha = 8°$ $\alpha = 10°$

NACA

L-70795

Figure 11.- Liquid-film pictures of wing upper surface at $R = 1.04 \times 10^6$.

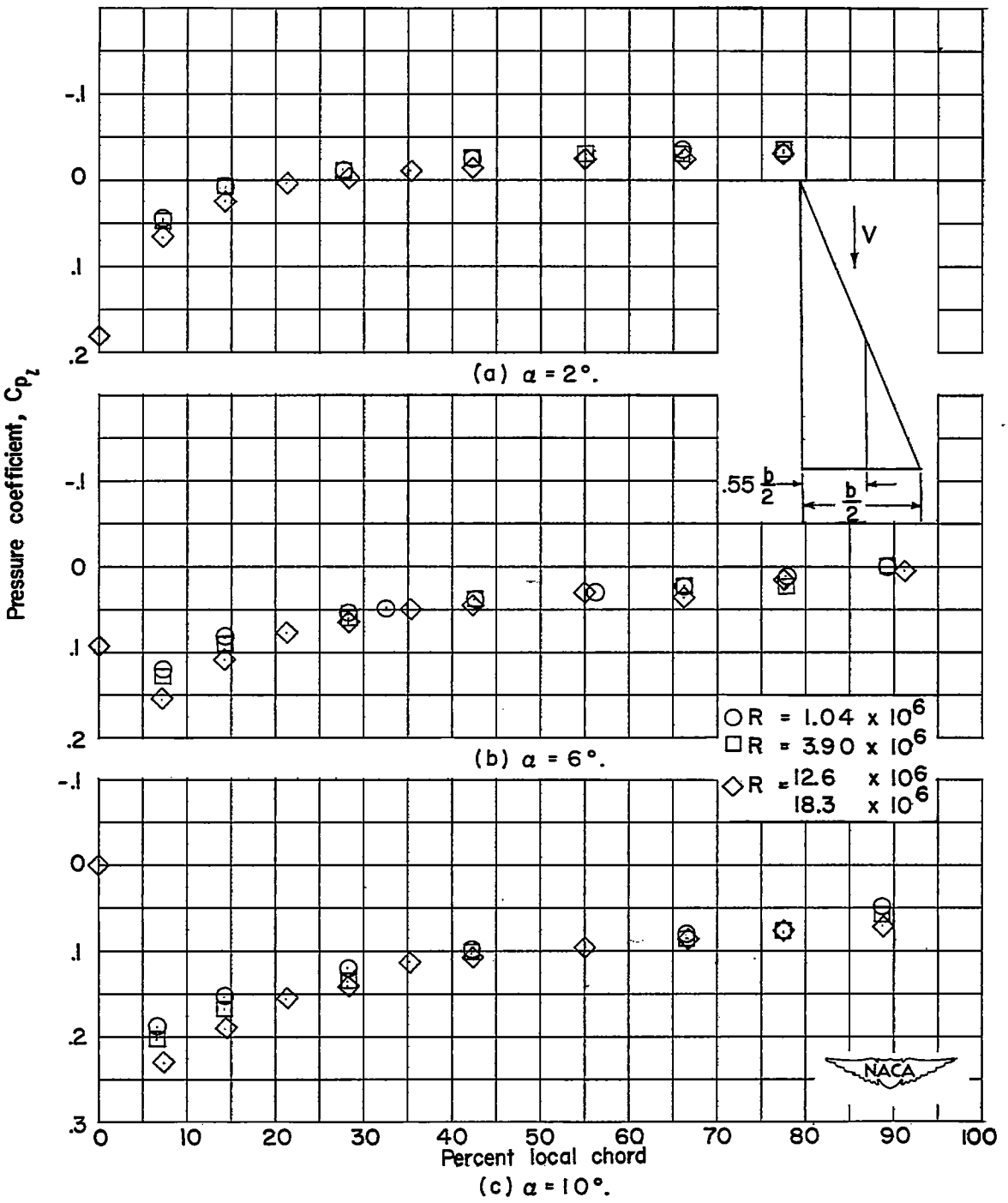

Figure 12.- Chordwise variation of lower-surface pressure coefficient at 0.55b/2 at different Reynolds numbers.

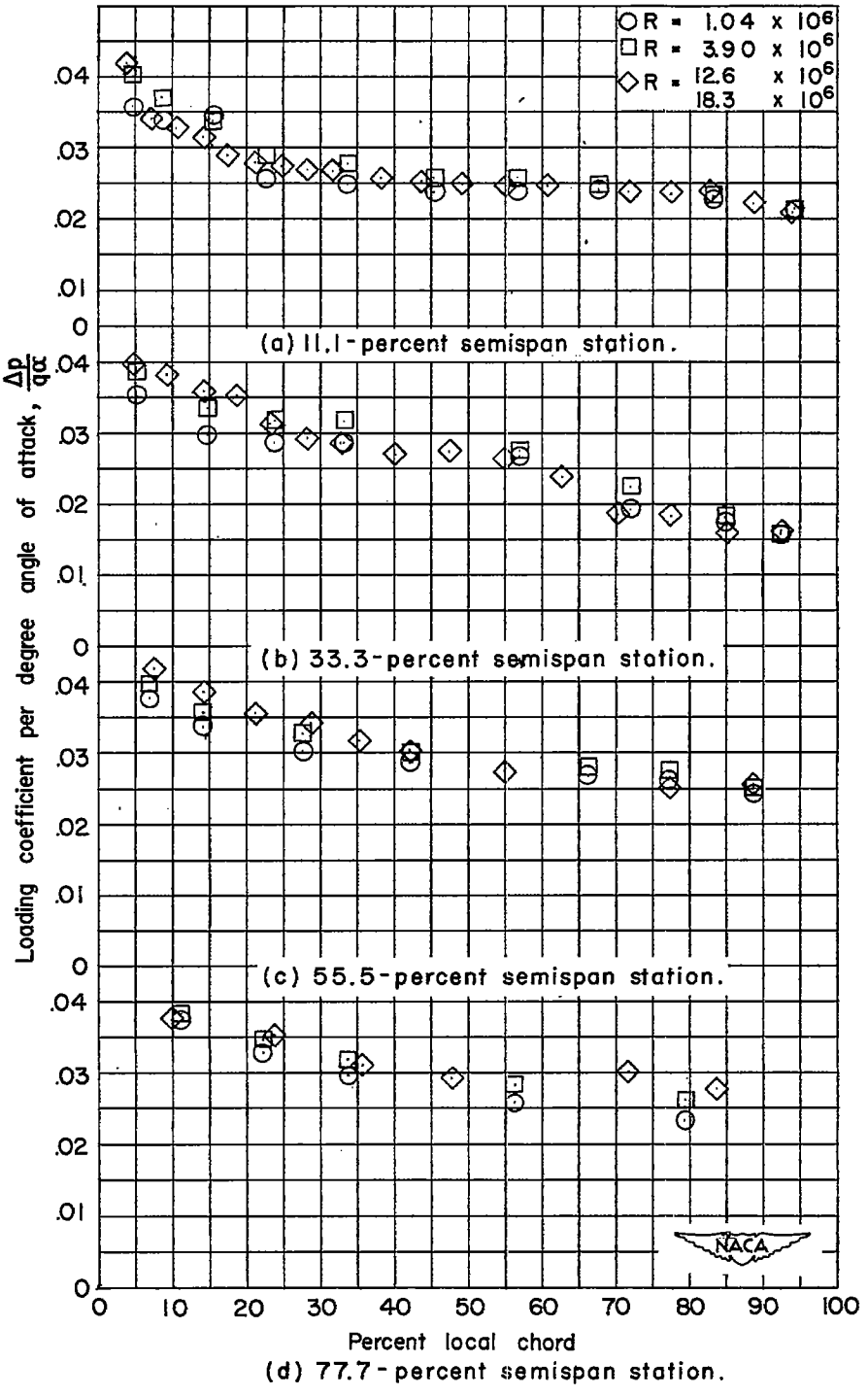

Figure 13.- Chordwise variation of wing loading coefficient at different Reynolds numbers for $\alpha = 10^{\circ}$.

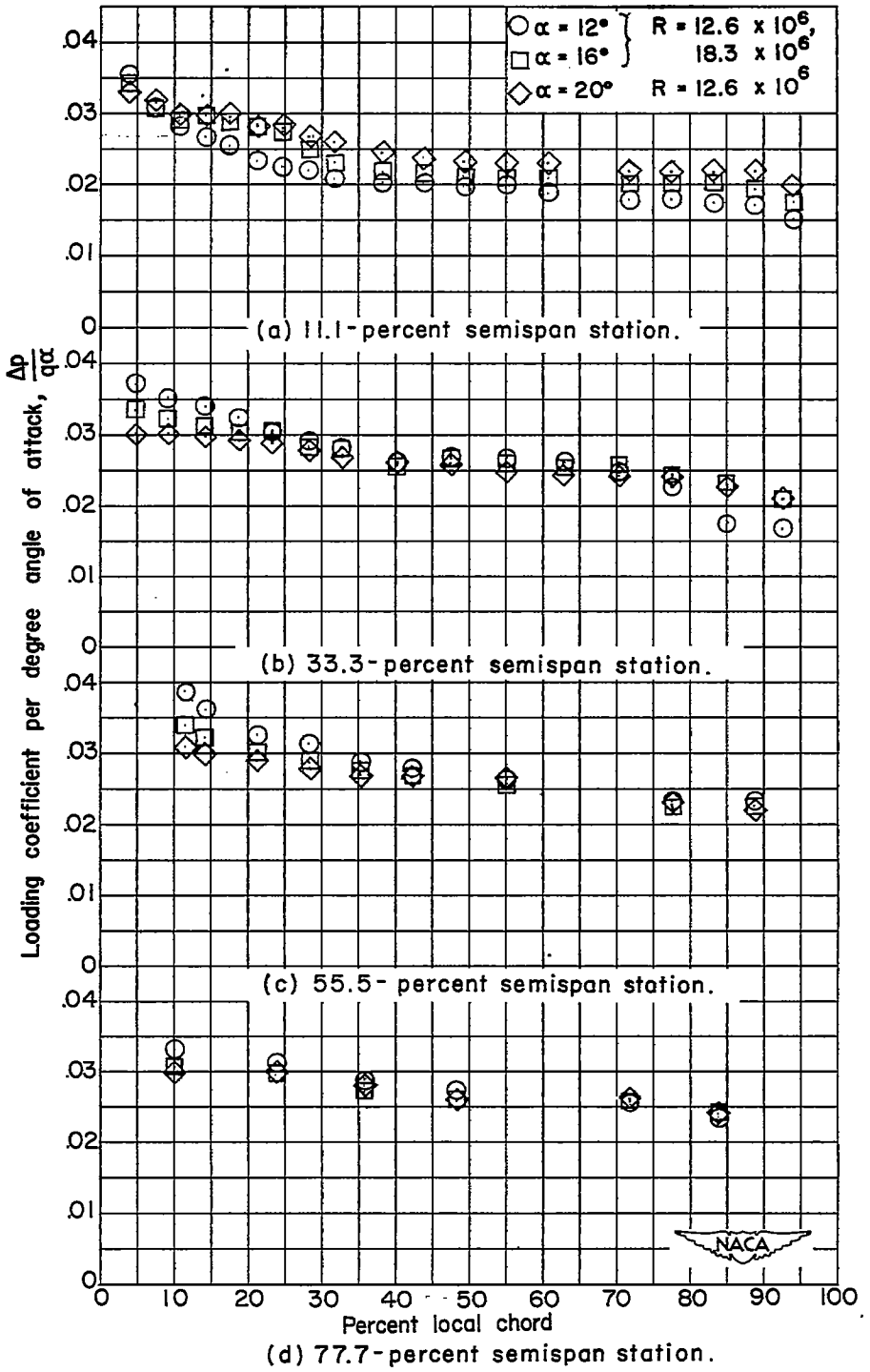

Figure 14.- Chordwise variation of wing loading coefficient at high angles of attack at Reynolds numbers of 12.6×10^6 and 18.3×10^6.

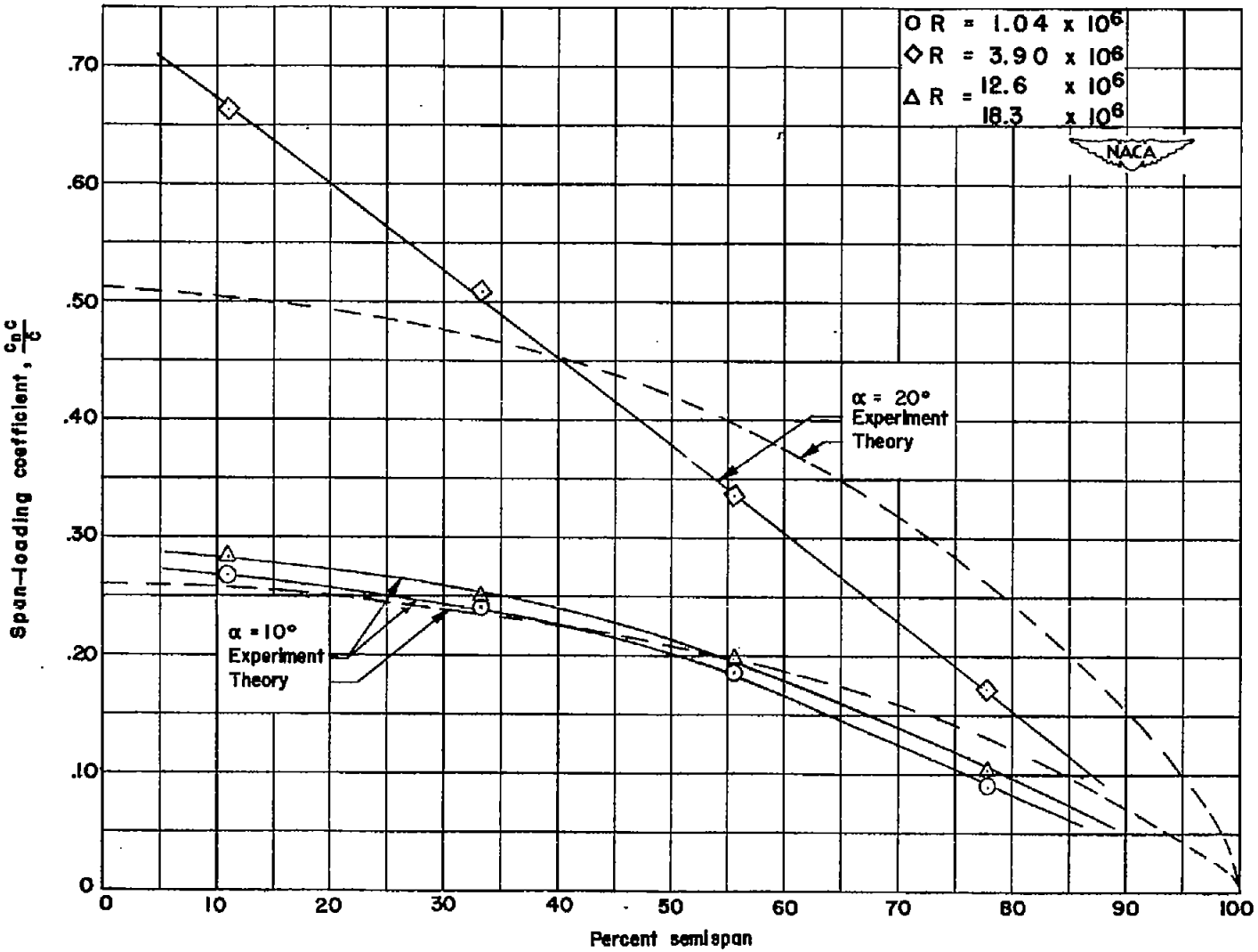

Figure 15.- Comparison of theoretical and experimental spanwise load distribution at different Reynolds numbers.